The Astrophysical Journal, 675:1194–1212, 2008 March 10

BARS IN DISK-DOMINATED AND BULGE-DOMINATED GALAXIES AT $z \sim 0$: NEW INSIGHTS FROM ~3600 SDSS GALAXIES

Fabio D. Barazza,[1] Shardha Jogee, and Irina Marinova
Department of Astronomy, University of Texas at Austin, 1 University Station C1400, Austin, TX 78712-0259;
barazza@astro.as.utexas.edu, sj@astro.as.utexas.edu, marinova@astro.as.utexas.edu
Received 2007 May 26; accepted 2007 October 23

ABSTRACT

We present a study of large-scale bars in the local universe, based on a large sample of 3692 galaxies, with $18.5 \leq M_g < -22.0$ mag and redshift $0.01 \leq z < 0.03$, drawn from the Sloan Digitized Sky Survey. Our sample includes many galaxies that are disk-dominated and of late Hubble types. Both color cuts and Sérsic cuts yield a similar sample of ~2000 disk galaxies. We characterize bars and disks by ellipse-fitting *r*-band images and applying quantitative criteria. After excluding highly inclined (60°) systems, we find the following results. (1) The optical *r*-band fraction ($f_{\rm opt-r}$) of barred galaxies, when averaged over the whole sample, is ~48%-52%. (2) When galaxies are separated according to half light radius (r_e), or normalized r_e/R_{24}, which is a measure of the bulge-to-disk (B/D) ratio, a remarkable result is seen: $f_{\rm opt-r}$ rises sharply, from ~40% in galaxies that have small r_e/R_{24} and visually appear to host prominent bulges, to ~70% for galaxies that have large r_e/R_{24} and appear disk-dominated. (3) For galaxies with bluer colors, $f_{\rm opt-r}$ rises significantly (by ~30%). A weaker rise (by ~15%–20%) is seen for lower luminosities or lower masses. (4) While hierarchical ΛCDM models of galaxy evolution models fail to produce galaxies without classical bulges, our study finds that ~20% of disk galaxies appear to be "quasi-bulgeless." (5) We outline how the effect of a decreasing resolution and a rising obscuration of bars by gas and dust over $z = 0.2$–1.0 can cause a significant artificial loss of bars, and an artificial reduction in the optical bar fraction over $z = 0.2$–1.0.

Subject headings: galaxies: bulges — galaxies: evolution — galaxies: general — galaxies: structure

1. INTRODUCTION

The majority (~60%) of bright disk galaxies are barred when observed in the near-infrared (Knapen 1999; Eskridge et al. 2000; Laurikainen et al. 2004; Menéndez-Delmestre et al. 2007; Marinova & Jogee 2007, hereafter MJ07), and a significant fraction of these (~45%) also appear barred in the optical (Eskridge et al. 2000; MJ07). Earlier studies suggested a striking or order-of-magnitude decline in the optical fraction of bars out to $z \sim 1$ (Abraham et al. 1999; van den Bergh et al. 2000), but subsequent studies have ruled out an order-of-magnitude decline and find that the optical fraction of strong bars remains fairly constant or show a moderate decline of a factor of ~2 (Jogee et al. 2004; Elmegreen et al. 2004a; Zheng et al. 2005; Sheth et al. 2003, 2004; 2007; see § 6).

Bars are believed to be very important with regard to the dynamical and secular evolution of disk galaxies, particularly in redistributing the angular momentum of the baryonic and dark matter components of disk galaxies (Combes & Sanders 1981; Weinberg 1985; Combes et al. 1990; Debattista & Sellwood 2000). The interaction between the bar and the disk material can lead to the inflow of gas from the outer disk to the central parts, which can trigger starbursts (Elmegreen 1994; Knapen et al. 1995; Regan & Teuben 2004; Jogee et al. 2005; Sheth et al. 2005) and might contribute to the formation of disky bulges (or "pseudobulges"; Kormendy 1993; Kormendy & Kennicutt 2004; Athanassoula 2005; Jogee et al. 2005; Debattista et al. 2006). Additional evidence for secular evolution is provided by box- or peanut-shaped bulges in inclined galaxies. These features are commonly attributed to the orbital structure, resonances, and vertical instabilities in a barred potential (Combes et al. 1990; Kuijken & Merrifield 1995; Bureau & Freeman 1999; Bureau & Athanassoula 2005).

From a theoretical perspective, it is possible to model some aspects of the evolution of disks and bars, and their interactions (e.g., the corresponding simulations are able to reproduce certain broad features of barred disks). However, it remains unclear why a specific galaxy has a bar, but a seemingly similar galaxy is unbarred; or why some barred galaxies have a classical bulge, whereas others harbor a disky bulge, etc. This might indicate that specific properties of the disks or the particular processes involved in their formation have a strong impact on their ability to form a bar. In order to investigate how disk and bar formation are related, it is not only important to determine the fraction of disk galaxies that are barred, but also to relate bar and disk properties. There are different methods to find and characterize bars. The Third Reference Catalog of Bright Galaxies (de Vaucouleurs et al. 1991, hereafter RC3) uses three bar strength families (SA, SAB, and SB) to characterize bars based on a visual inspection of blue light images. Using this classification Odewahn (1996) showed that the optical fraction of strong bars in disk galaxies rises from Sc galaxies toward later types. More quantitative measures, such as the gravitational torque method (Block et al. 2002; Laurikainen et al. 2002; Buta et al. 2005), or Fourier dissection (Buta et al. 2006; Laurikainen et al. 2006), were also used, not only to find bars, but to quantitatively determine bar strengths and bar lengths. Similarly, the method of fitting ellipses to galaxy isophotes provides a tool to characterize the length and shape of bars (Friedli et al. 1996; Jogee et al. 1999, 2002a, 2002b; Knapen et al. 2000; Sheth et al. 2000, 2003, 2007; Laine et al. 2002; Whyte et al. 2002; Elmegreen et al. 2004a; Reese et al. 2007; Marinova & Jogee 2007; Menéndez-Delmestre et al. 2007).

These efforts were able to shed light on the fraction, shapes, and structures of bars in local disk galaxies of early to intermediate Hubble types. First attempts were made to relate the presence of a bar or its structural properties to other galaxy characteristics. However, there were three important limitations. First, samples used in earlier studies were small (~100–200 objects) and mostly

[1] Current address: Laboratoire d'Astrophysique, École Polytechnique Fédérale de Lausanne (EPFL), Observatoire, CH-1290 Sauverny, Switzerland.

composed of bright galaxies of early to intermediate Hubble types (Sa to Sc), with fairly prominent bulges. One could barely get decent number statistics for bars in early-type disk galaxies, while the bins of disk-dominated late Hubble types were dominated by Poisson noise (e.g., see Fig. 16 in MJ07). Second, with such small samples, it was difficult to bin galaxies in terms of the galaxy host properties. Third, earlier samples were drawn from a very small volume, and could be highly impacted by cosmic variance.

In the present study, we use a sample of ~2000 galaxies, at $z = 0.01$–0.03 with $M_r \sim -18.5$ to -22.0 mag. The first advantage of this study is that it provides a factor of 10 improvement in number statistics and reduces the effect of cosmic variance by selecting galaxies drawn from a larger volume. Second, with ~2000 galaxies, we can for the first time have 100–200 galaxies per bin, while binning galaxies in terms of host galaxy parameters, such as luminosity, measures of bulge-to-disk (B/D) ratios, size, colors, surface brightness, etc. This allows us to conduct a comprehensive study of barred and unbarred galaxies as a function of host galaxy properties. Third, our sample has a large number of galaxies, which are relatively faint ($M_g > -19.5$ mag) or/and appear disk-dominated, characteristic of late Hubble types. This allows us to shed light on what happens to bars at the fainter end of the luminosity function and in the regime of disk-dominated galaxies.

A fourth goal of our study is to provide a reference baseline for bars at $z \sim 0$ in the *rest-frame optical* for intermediate-redshift *HST* surveys using the Advanced Camera for Surveys (ACS), such as the Tadpole field (Tran et al. 2003), the Galaxy Evolution from Morphologies and SEDs (GEMS, Rix et al. 2004), the Great Observatories Origins Deep Survey (GOODS, Giavalisco et al. 2004), and COSMOS (Scoville et al. 2007), which trace bars in the rest-frame optical band at $z \sim 0.2$–1.0 (look-back times of 3–8 Gyr). We use SDSS to provide the reference point at $z = 0$ in the r-band, complementing the one in the B-band of MJ07. Our B- and r-band results can be directly compared to *HST* ACS optical studies of bars in bright disks at $z \sim 0.2$–1.0 (Elmegreen et al. 2004a; Jogee et al. 2004). The validity of this comparison is reinforced by the fact that we use the same procedure of ellipse fits (§ 3) that were used by these studies. We also note that the reference $z = 0$ point for bars in the near-infrared band (Menéndez-Delmestre et al. 2007) is not appropriate for comparison with the above *HST* ACS surveys, which trace the rest-frame optical rather than the rest-frame near-infrared.

The outline of the paper is as follows: In § 2 we present our sample selection. The method used to find and characterize bars is explained in § 3. In § 4 we discuss the detection limits. Our results and more detailed assessments of specific findings are presented in § 5. We discuss our results in § 6 and summarize our conclusions in § 7. Throughout the paper we assume a flat cosmology with $\Omega_M = 1 - \Omega_\Lambda = 0.3$ and $H_0 = 70$ km s^{-1} Mpc^{-1}.

2. SAMPLE SELECTION

Our sample of local disk galaxies is drawn from the low-redshift catalog of the New York University Value-Added Catalog (NYU-VAGC; Blanton et al. 2005). The NYU-VAGC is based on the second data release of SDSS, which is acquiring *ugriz* CCD imaging of 10^4 deg^2 of the northern Galactic sky and selecting 10^6 targets for spectroscopy, most of them galaxies with $r < 17.77$ mag (Abazajian et al. 2004). The low-redshift catalog consists of 28089 galaxies at distances of 10–200 Mpc ($0.0033 < z < 0.05$), which have been determined by correcting for peculiar velocities. For each galaxy, background-subtracted and deblended images in *ugriz*, as well as individual PSF frames, are available.

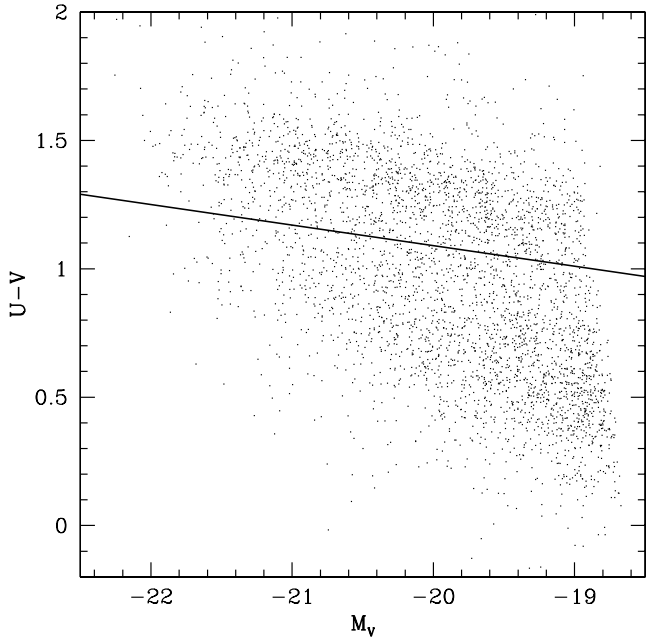

FIG. 1.—Color-magnitude diagram of our initial sample of 3692 galaxies. The solid line corresponds to $U - V = 1.15 - 0.31z - 0.08[M_V - 5\log(h) + 20]$ (Bell et al. 2004a). The blue galaxies lying below this line (1961 objects) are included in our sample of local disk galaxies.

We selected galaxies in the redshift range $0.01 < z < 0.03$, having $M_g \leq -18.5$ mag. The typical seeing (1.4″) corresponds to 290–840 pc over $0.01 \leq z < 0.03$. This is adequate for resolving large-scale bars, which are the focus of this study. Large-scale bars have diameters ≥2 kpc and their lengths encompass at least 2.5 independent PSFs, allowing them to be resolved and fitted. We note that bars with diameters below 2 kpc or semi major axis $a_{\rm bar} < 1$ kpc are typically considered as nuclear rather than large-scale bars (Laine et al. 2002). Nuclear bars are not the focus of this study and are excluded from our results. Hence, it is not a source of concern, if some of them are unresolved by the data. The selected sample is complete down to $M_g \leq -18.5$ mag in the chosen redshift range and consists of 3692 objects. The magnitude distribution covers $M_r = -18.5$ to -22.0 mag (Fig. 1).

We use the GALFIT (Peng et al. 2002) software to perform single-component Sérsic fits of the form

$$\Sigma(r) = \Sigma_e \exp\left\{-\kappa\left[\left(\frac{r}{r_e}\right)^{1/n} - 1\right]\right\}$$

to the two-dimensional images, which provide Sérsic indices (n) and half-light radii (r_e) for the galaxies; Σ_e is the pixel surface brightness at r_e, and κ is a dependent variable and coupled to n.

The optical bar fraction is defined as the fraction of disk galaxies that host large-scale bars, hence we must first define a sample of disk systems. There are two common methods to separate disks and elliptical galaxies. For giant galaxies, the first method is to use the Sérsic index from single-component fits and define giant disk galaxies to have $n < 2.5$ (e.g., Jogee et al. 2004; Bell et al. 2004b; Barden et al. 2005). The second method is to apply a color cut defined in color-magnitude space (e.g., Bell et al. 2004b; McIntosh et al. 2005; Wolf et al. 2005), assuming that disk galaxies are predominantly bluer, star-forming systems. Both methods have limitations. The color cut may miss out disk systems that are red due to the presence of a dusty starburst. The Sérsic cut may be contaminated by some bright and rather blue dwarf ellipticals

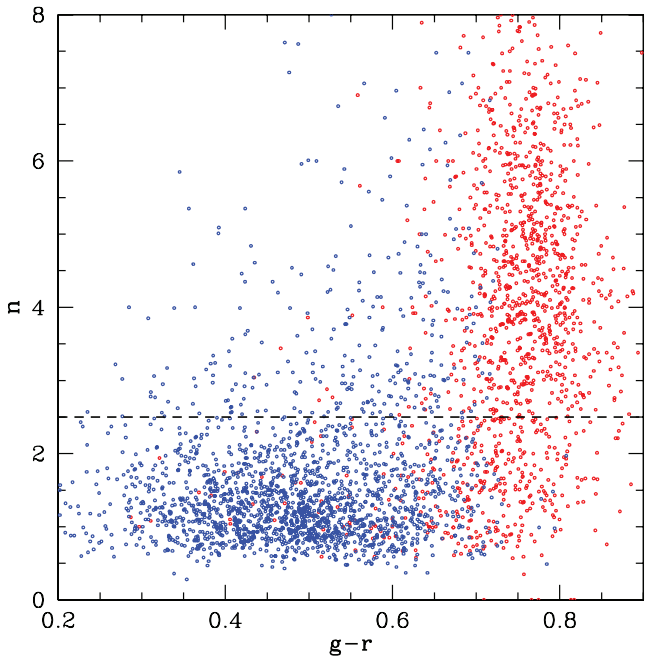

FIG. 2.—Comparison of the subsamples based on Sérsic and color cuts. The $g-r$ color is plotted vs. the Sérsic index n. In the subsample based on a color cut, the galaxies represented by blue dots are selected, while the red dots are excluded. The subsample based on a Sérsic cut $n < 2.5$ lie below the dashed line. Blue galaxies below the line belong to both subsamples. Notice the strong overlap between the two subsamples.

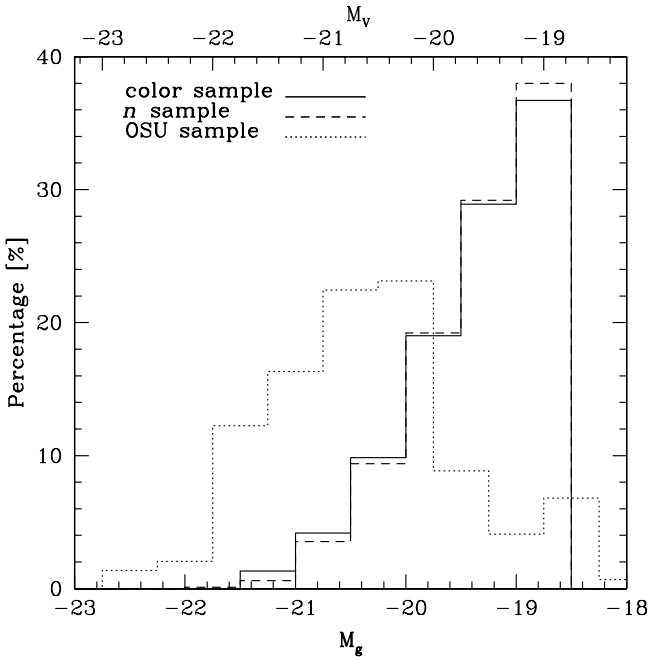

FIG. 3.—Distribution of absolute magnitudes is shown for our subsamples of disk galaxies based on Sérsic and color cuts, and, as comparison, for the OSUBSGS disk sample. For the latter we show M_V, which is given on the upper axis. The strong dominance of fainter galaxies in the SDSS samples is evident.

and miss out certain galaxies with point-like AGN sources. We applied both methods to our sample as illustrated in Figure 1 and 2. The corresponding disk samples have an overlap of ∼85% (Figs. 2 and 3). In Figure 2 the color-selected and Sérsic-selected samples are plotted in the $g-r$ versus n plane, with the color-selected galaxies in blue, and the good overlap is evident. Figure 3 shows the similar magnitude distributions of the color-selected and Sérsic-selected disk samples from SDSS. Figure 3 also illustrates a crucial property of the SDSS disk sample. The sample covers a magnitude range of ∼3 mag, but is clearly dominated by fainter galaxies ($M_r = -18.5$ to -20.0 mag). Furthermore, visual inspection shows that a large fraction of these galaxies seems to be disk-dominated, with little or no bulge visible. We do not have Hubble types for these SDSS galaxies, but these characteristics are typical of late-type galaxies (Sd, Sm). This is a crucial point and has to be kept in mind for the discussion of the results presented below. As discussed in § 1, such galaxies are underrepresented in most studies of bars in local disk galaxies carried out to date. As an illustration, the magnitude distribution in M_V of spirals in the OSU Bright Spiral Galaxy Survey (OSUBSGS; Eskridge et al. 2002) is overplotted in Figure 3. This sample is often used as a reference sample for bars at $z = 0$ (e.g., Eskridge et al. 2000; Block et al. 2002; Whyte et al. 2002; Buta et al. 2005; MJ07).

We finally opted for the color cut, since the contamination of $n < 2.5$ objects in the sample is slightly smaller than the fraction of red sequence galaxies in the sample defined by $n < 2.5$. We applied the color cut $U - V < 1.15 - 0.31z - 0.08[M_V - 5\log(h) + 20]$ (Bell et al. 2004a), where $h = H_0/100$ and $h = 0.7$ is used in this paper. This cut is parallel to the red sequence in the color-magnitude diagram and stems from an empirical fit to the evolution of the color-magnitude relation for galaxy clusters at different redshifts. It therefore corresponds to a definition of the red sequence based on a number of nearby and distant clusters, but shifted by 0.25 mag to the blue. The color-magnitude diagram for our sample is shown in Figure 1. The solid line indicates the color cut. The resulting sample of disk galaxies contains 1961 objects.

The sample in this paper only includes galaxies in the redshift range $0.01 \leq z < 0.03$. For completeness, we mention that the analysis outlined in § 5 has also been performed on the 1890 galaxies in the redshift range $z = 0.03$–0.04, and yields essentially the same results. We did not include these galaxies in the sample of this paper because the seeing at $z \sim 0.04$ (1.4″ or 1.1 kpc) is in the limiting range where we can still resolve large-scale bars of diameter ≥2 kpc, but the fit may not be as robust.

3. CHARACTERIZATION OF BARS AND DISKS

The method used to find and characterize bars in disk galaxies is based on fitting ellipses to the isophotes on the r-band images of our sample galaxies, along with a set of quantitative criteria outlined below. We opted for the r-band, because it provides deeper images than observations in the other SDSS filters. Many observational studies have used and refined the method of fitting ellipses to characterize bars (Friedli et al. 1996; Jogee et al. 1999, 2002a, 2002b; Knapen et al. 2000; Sheth et al. 2000, 2003, 2007; Laine et al. 2002; Whyte et al. 2002; Elmegreen et al. 2004a; Reese et al. 2007; Marinova & Jogee 2007; Menéndez-Delmestre et al. 2007). There is also a strong body of theoretical evidence (Athanassoula 1992a; Shen & Sellwood 2004) supporting this approach, as outlined in MJ07. In particular, Athanassoula (1992a) studied orbits in analytic potentials of barred galaxies and showed that generalized ellipses are a good representation of the main bar-supporting stellar orbits. The departure of ellipses fitted by the IRAF task `ellipse` from these generalized ellipses is characterized by the value of the harmonic amplitudes A3, B3, A4, and B4, and we find that they are small (typically <10%).

When using ellipse fits to characterize bars and disks, we use the method and steps developed by Jogee et al. (2004) and described in detail in Jogee et al. (2004) and MJ07. In the following, we give a short description. We use the standard task `ellipse` to fit ellipses to the images out to a certain radius $a_{\max}$, which is determined to

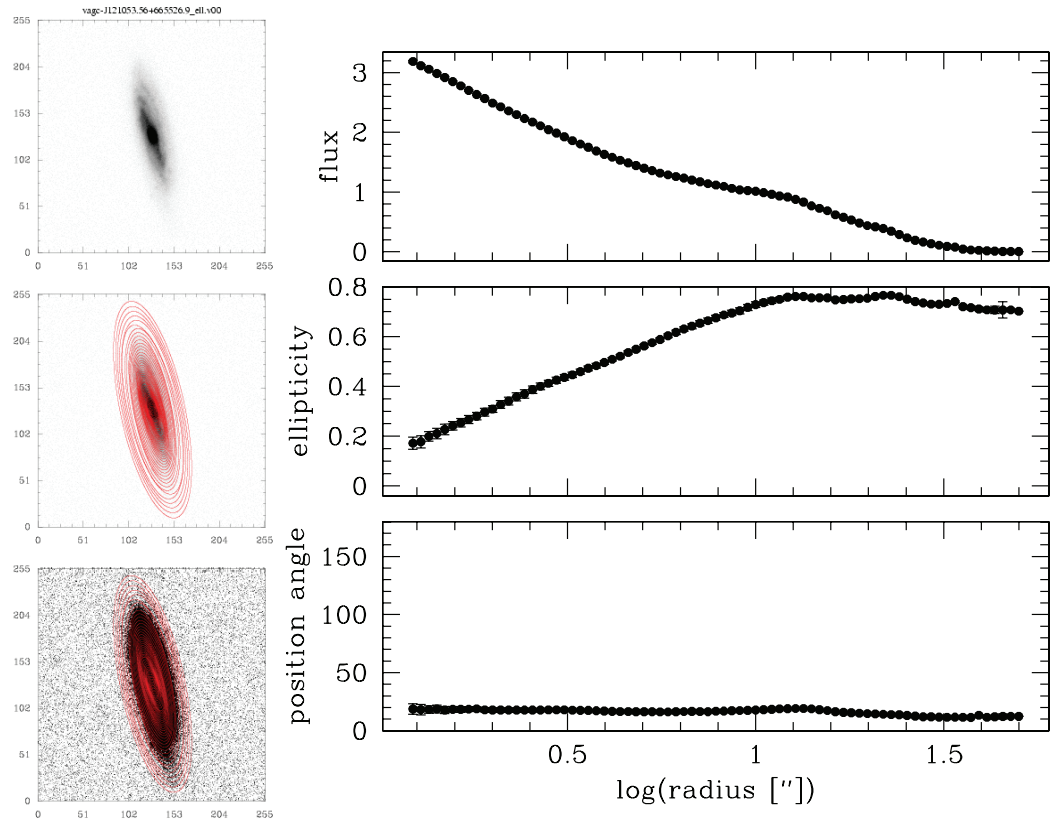

FIG. 4.—Example of an inclined ($i > 60^\circ$) galaxy, which is identified from the overlays and radial profiles generated by the ellipse fits. *Left*: The top image shows only the galaxy, while the middle and bottom images show the ellipses overlaid on the galaxy, with gray-scale stretches chosen to emphasize the inner (*middle image*) and outer (*bottom image*) regions of the galaxy. The images are roughly 100″ on a side. *Right*: The radial profiles of surface brightness (*top*), ellipticity e (*middle*), and P.A. (*bottom*) are shown. In the outer parts of the galaxy, the P.A. is flat and the ellipticity is fairly constant at $e > 0.5$, indicating that the galaxy has a large inclination $i > 60^\circ$.

be the radius where the galaxy isophotes reach the sky level. An iterative wrapper is used to run `ellipse` up to 300 times for each object in order to get a good fit across the whole galaxy. We performed ellipse fits for the subsample of 1961 disk galaxies defined by the color cut. For 101 ($\sim 5\%$) galaxies, no ellipses could be fitted, mainly due to the fact that the fitting routine could not find the galaxy center. This is typically the case for strongly disturbed galaxies, or on images where a foreground object was not properly removed. In both cases, the surface brightness of the galaxies is not steadily decreasing from the center toward larger radii, but is rather oscillating between higher and lower values impeding a proper ellipse fit. The remaining 1860 galaxies have then been classified in the way described below. From the best fit for each galaxy, we plot the associated radial profiles of surface brightness (SB), ellipticity (e), and position angle (P.A.). Furthermore, the fitted ellipses are overplotted onto the galaxy images to generate overlays. Examples of the radial profiles and the overlays are shown in Figures 4, 6, and 7. During the classification process, the plots, the images, and overlays of the fitted ellipses onto the images, are displayed using an interactive visualization tool (Jogee et al. 2004), and used to classify a galaxy as "inclined," "barred," or "unbarred." We use the ellipticity in the outer disk to estimate the inclination i. We adopt the standard procedure of excluding all objects with an inclination $i > 60^\circ$, as morphological and structural analysis are unreliable in highly inclined galaxies. Figure 4 shows an example of such a case. We find 648 galaxies ($\sim$35%) with $i > 60^\circ$. In Figure 5 we show the luminosity and color distributions of the galaxies with $i > 60^\circ$ compared to the ones with $i < 60^\circ$. The distributions in terms of absolute magnitude are very similar, whereas the more inclined galaxies tend to be redder than the more face-on objects. This is expected due to the dust extinction in the disks.

In the next step, we classify the galaxies with $i < 60^\circ$ as unbarred or barred, based on the following quantitative criteria: (1) the ellipticity increases steadily to a global maximum greater than 0.25, while the P.A. value remains constant (within 10°), and (2) the ellipticity then drops by at least 0.1 and the P.A. changes at the transition from the bar to the disk region (Figs. 6 and 7 show examples of a barred and unbarred galaxy, respectively). Criterion 1 is based on the fact that in the region where bars are dominated by the "x_1" family of periodic stellar orbits (Contopoulos & Papayannopoulos 1980), we expect the ellipses to be aligned along the bar P.A. and to become increasingly eccentric toward the end of the bar. Therefore, the ellipticity should reach a global maximum and the P.A. should not fluctuate strongly. This is intuitively evident from the fact that bars appear morphologically as linear elliptical features centered on the galaxy. The requirement that the P.A. must remain constant in the bar region is important for excluding other features, such as spiral arms that may have a high global ellipticity. Criterion 2 is applied, because the disks are mostly more circular than the bar for moderately inclined galaxies and the disk and bar have different P.A. in general. After having classified a galaxy, we use the interactive display tool to measure the ellipticity, P.A., and semimajor axis of its outer disk. For galaxies classified as barred we measure the same quantities, as well as the maximum ellipticity, $e_{\rm bar}$, of the bar and the radius, $r_{{\rm max}e}$, of maximum bar ellipticity. We use $e_{\rm bar}$ as a partial measure of the bar strength and the radius $r_{{\rm max}e}$ as an estimate for the semimajor axis of the bar. A detailed theoretical and empirical justification of this approach is provided in Jogee et al. (2004) and MJ07.

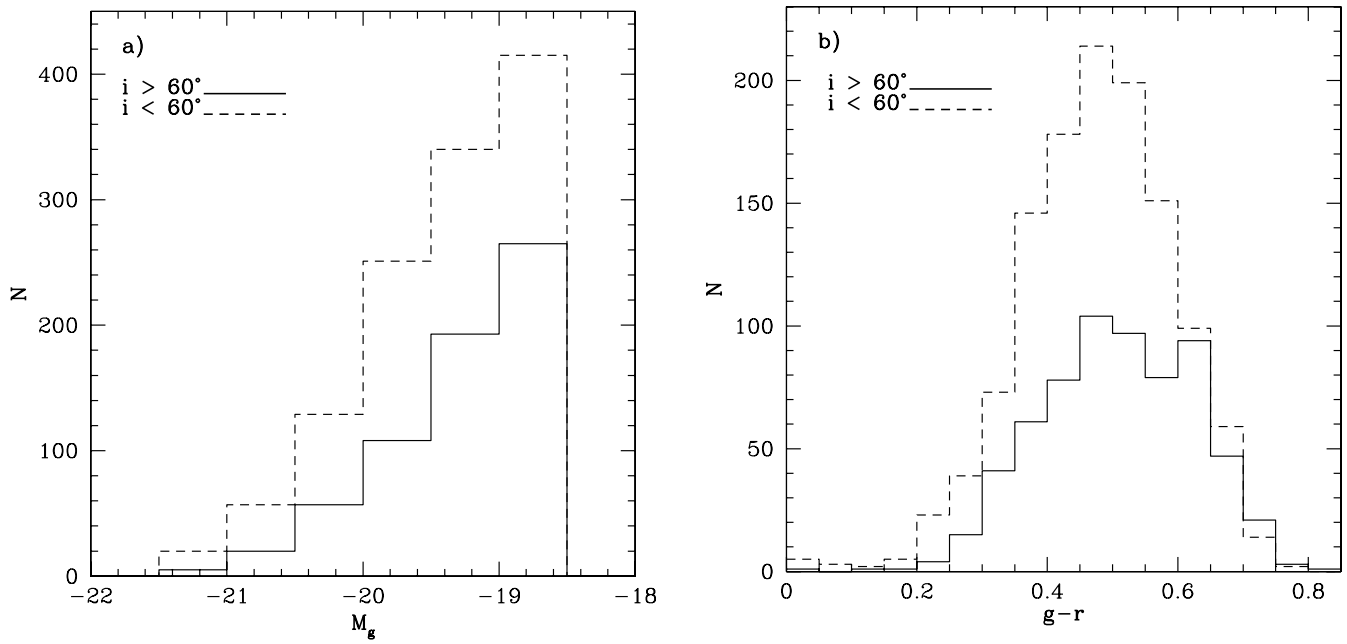

FIG. 5.—(*a*) The absolute magnitude distributions of galaxies with $i > 60^{\circ}$ (*solid line*) compared to the ones with $i < 60^{\circ}$ (*dashed line*). (*b*) The corresponding color distribution, showing the stronger effect of dust extinction in more inclined disks.

Some of the galaxies exhibit all features required to be classified as barred, except the "constant P.A." criterion, i.e., their P.A. twists. These galaxies are classified as "twisted," but regarded as unbarred. However, some of these galaxies could be weakly barred, since in weak bars the dust lanes on the leading edge of the bar are curved (Athanassoula 1992b), which could cause an isophotal twist. The number of such objects is not very high (∼7%) and therefore they do not significantly affect the results.

We note that the classifications and the measurements of sizes, ellipticities, and so on are performed on the *observed* images and

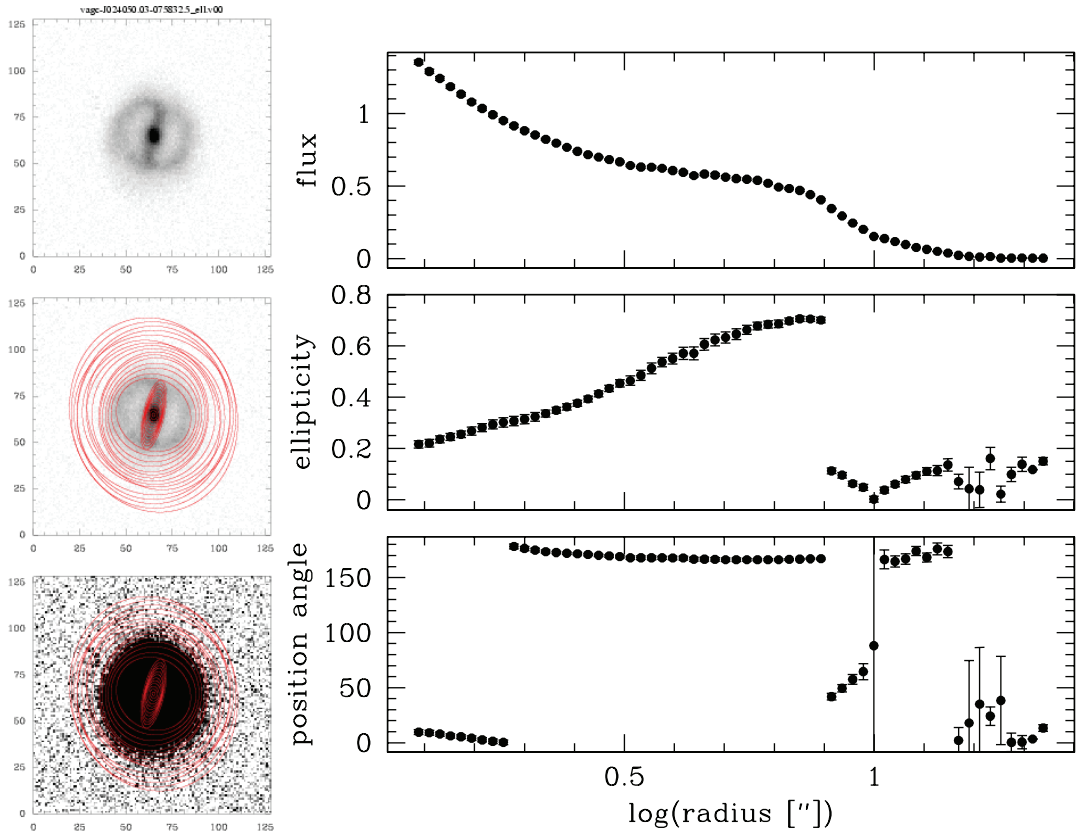

FIG. 6.—Same as Fig. 4, but for a galaxy classified as barred from the ellipse fits. The images on the left are roughly 50″ on a side. Over the bar region, *e* rises smoothly to a global maximum of ∼0.7, while the P.A. remains ∼constant. After the bar end, as we transition to the more circular disk, the ellipticity drops sharply at ∼8″ and the P.A. changes significantly at this point.

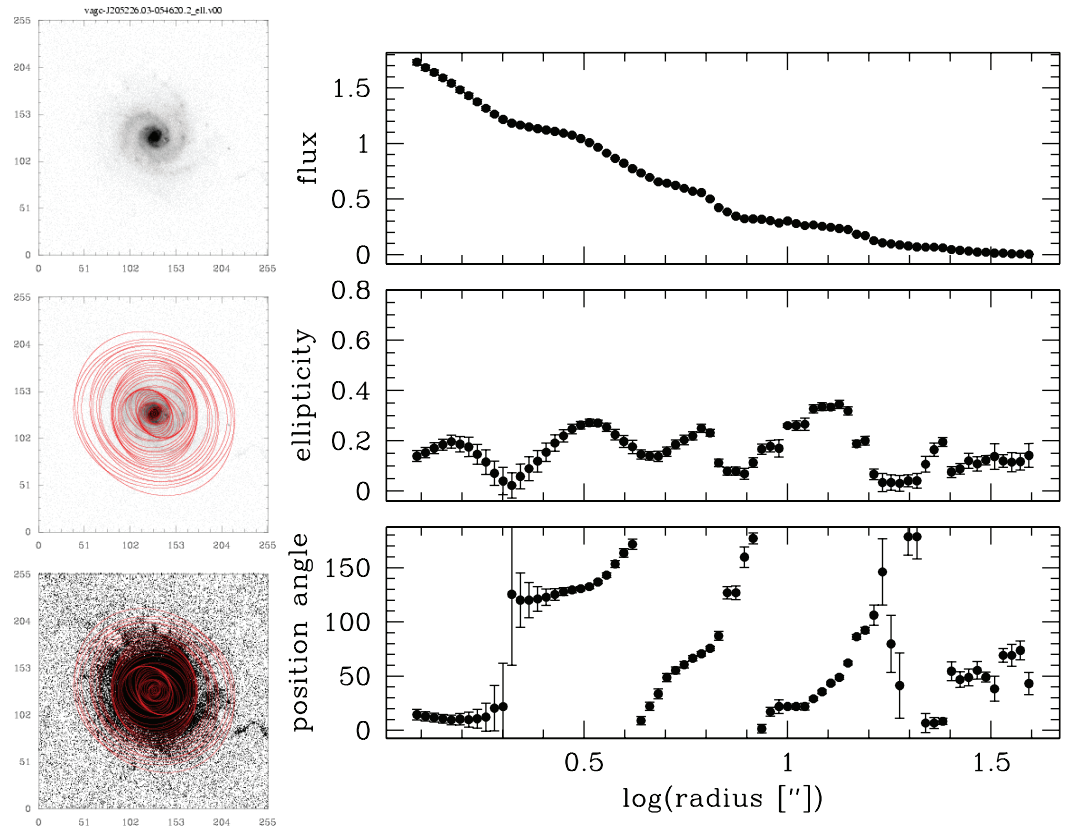

FIG. 7.— Same as Fig. 4, but for a galaxy classified as unbarred. The images on the left are roughly 100″ on a side. Here, no bar signature is evident. Instead the ellipticity profile oscillates and the P.A. twists due to the spiral structure in the disk.

profiles, which are affected by projection effects. We did not attempt to deproject our galaxies, since it is difficult to determine the P.A. in the outer disks accurately enough, in order to obtain a reliable deprojection. This is particularly true for disks with ellipticities $e_{\rm disk} < 0.2$, for which the uncertainty of the P.A. determination can reach up to 30°–40° in our data. Furthermore, MJ07 have shown that the statistical results before and after deprojecting their galaxies are very similar. Finally, we note that our undeprojected results can be directly compared with studies of barred galaxies at intermediate redshifts, where deprojection has not been carried out (Jogee et al. 2004; Elmegreen et al. 2004a; Zheng et al. 2005).

Out of our sample of 1860 disk galaxies, we find 553 to be barred, 591 to be unbarred (including 76 classified as twisted), and 648 to be too inclined ($i > 60^\circ$). We did not classify the remaining 68 galaxies for the following reasons. For 30 galaxies, the ellipse fits obviously failed or the profiles were extremely messy: this occurred when foreground/background objects were not completely removed or for galaxies with very low surface brightnesses and very irregular shapes. The other 38 galaxies were ambiguous cases where deprojection might make a large difference. Specifically, in these galaxies, the ellipticity rises smoothly to a *local* maximum while the P.A. stays relatively constant, but this maximum ellipticity is less than that of the outer disk. In such cases, deprojection may turn the local maximum into a global maximum, particularly if the bar is perpendicular to the line of nodes. These objects are further discussed in § 4.

In Table 1 we give the median values of the basic properties for the barred, unbarred, inclined, and unclassifiable objects.

4. DETECTABILITY OF BARS

When using optical images, the obscuration of bars by dust and star formation can prevent their unambiguous detection. Comparing the results of quantitative bar studies conducted in the optical and in the near-infrared, shows that the near-IR bar fraction can be a factor of ∼1.3 higher than in the optical (e.g., Marinova & Jogee 2007; Menéndez-Delmestre et al. 2007). It is therefore clear that we miss bars due to dust extinction and that our bar fraction has to be considered as a lower limit. Furthermore, our results can only be compared to studies, which have also been performed using observations in the optical.

Apart from dust, the ability to detect a bar in a galaxy depends on its distance, its inclination, the angle θ between the line of nodes and the P.A. of the bar, as well as on the point-spread function (PSF) or seeing of the images used. We discuss each of these

TABLE 1
BASIC PROPERTIES OF THE SUBSAMPLES, RESULTING FROM THE CLASSIFICATION OF THE 1860 COLOR-SELECTED GALAXIES

Property	Barred	Unbarred	Too Inclined ($i > 60^\circ$)	No Class
Number	553	591	648	68
Percentage	29.7	31.8	34.8	3.6
$\langle M_g \rangle$ (mag)	−19.23	−19.27	−19.12	−19.50
$\langle g - r \rangle$ (mag)	0.48	0.49	0.51	0.49
$\langle z \rangle$	0.025	0.026	0.025	0.025
$\langle r_{\rm eff} \rangle$ (kpc)	4.13	3.12	4.63	4.62
$\langle n \rangle$	1.40	1.52	1.18	1.43

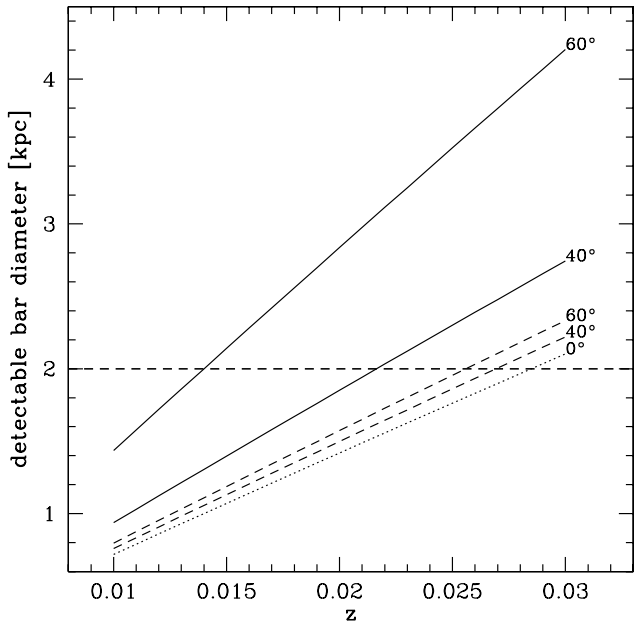

FIG. 8.—Horizontal line corresponds to the minimum bar diameter (2 kpc) of large-scale bars. The five diagonal lines show the smallest measurable bar diameter $d_{\rm min}$ as a function of redshift, for different values of the angle θ between the bar P.A. and the galaxy's lines of nodes, and for different inclinations i. When computing $d_{\rm min}$, we assume that a bar is detectable only if its diameter can encompass at least 2.5 times the PSF (1.4″) of the images. The two solid lines show the detection limit for the worst case scenario of $\theta = 90^\circ$, and two inclinations ($i = 40^\circ$ and 60°). The two dashed lines show the detection limit for a more moderate $\theta = 30^\circ$. The dotted lines shows the detection limit for the face-on case, where independent of θ, bars with diameters $\gtrsim$2 kpc are detectable out to $z = 0.03$.

factors below. The largest allowed inclination in our sample is $i = 60^\circ$. When computing the smallest measurable bar diameter $d_{\rm min}$, we assume that a bar is detectable only if its diameter can encompass at least 2.5 times the PSF (1.4″) of the images. The median seeing or PSF of the r-band images from SDSS is 1.4″, which corresponds to ~290 pc at $z = 0.01$ (our lower redshift limit) and to ~840 pc at $z = 0.03$ (our upper redshift limit). If a bar, which would be detectable in a face-on disk, happens to be perpendicular to the line of nodes in an inclined disk (i.e., $\theta = 90^\circ$), projection effects will reduce its apparent length and ellipticity compared to the intrinsic value, and this length may fall below the detection limit. For values of θ below 90°, these effects are less severe.

The variation of the detection limit $d_{\rm min}$ as a function of θ, i, and z is shown by the five diagonal lines in Figure 8. The horizontal line corresponds to the minimum bar diameter (2 kpc) of large-scale bars, and ideally, we want the detection limit to lie below this line at all redshifts. The two solid diagonal lines indicate the detection limits as a function of redshift for two different inclinations ($i = 40^\circ$ and $i = 60^\circ$) and the worst case scenario of $\theta = 90^\circ$. In that case, with $i = 40^\circ$ and $\theta = 90^\circ$, we start missing the smallest large-scale bars at $z > 0.02$. The two dashed diagonal lines on Figure 8 represent the detection limits for a more moderate θ of 30°. In that case, with $i = 40^\circ$ and $\theta = 30^\circ$, we start missing the smallest large-scale bars at $z > 0.027$. Finally, the dotted diagonal line on Figure 8 represents the face-on case ($i = 0^\circ$), where, independent of θ, bars with diameters $\gtrsim$2 kpc are detectable out to $z = 0.03$.

In Figure 9 we plot histograms of the absolute bar diameters in three different redshift bins and for the whole sample (the bin boundaries have been chosen in order to obtain roughly the same number of objects per bin). The vertical lines indicate our bar diameter limit of 2 kpc. Figure 9 shows that we do not miss significant numbers of small bars with increasing redshift. We find roughly the same number of bars with $2 < d_{\rm min} < 3$ kpc in the lowest and in the highest redshift bins.

In order to gauge the impact of projection effects on the derived bar ellipticities, we plot the distributions of barred and unbarred galaxies as a function of disk ellipticity in Figure 10*a*. The cutoff at disk ellipticities ($e_{\rm disk}$) at 0.5 is due to the fact that highly inclined disks with $i > 60^\circ$ are discarded from our sample (§ 3). As $e_{\rm disk}$ varies from 0 to 0.5, the total number of barred objects decreases only slightly at $e_{\rm disk} \gtrsim 0.3$. This fall could be attributed to two related factors. For a feature to be classified as a bar, our criterion (1) in § 3 requires its maximum ellipticity to reach a *global* maximum, which is higher than the ellipticity $e_{\rm disk}$ of the outer disk. At high inclinations, where $e_{\rm disk}$ is high, this criterion may not be satisfied even if the feature is truly a bar. Some of the 38 "unclassifiable" galaxies that we discussed at the end of § 3 fall in this category. A second factor is that if θ is close to 90°, then at high inclination i or $e_{\rm disk}$, the bar ellipticity is lowered significantly, making it fail criterion 1. However, it is clear from Figure 10*a*, that the number of bars we might miss in the two highest ellipticity bins ($\epsilon \gtrsim 0.3$) is not very high.

The distribution of bar ellipticities ($e_{\rm bar}$) in disks of different ellipticities ($e_{\rm disk}$) is shown in Figure 10*b*. The vertical line at $e_{\rm disk} = 0.5$ indicates the exclusion of highly inclined disks. The diagonal solid line is defined by $e_{\rm disk} = e_{\rm bar}$. All detected bars lie to the left of this line, reflecting the criterion (1) that the bar ellipticity $e_{\rm bar}$ must be a global maximum. We note that the maximum $e_{\rm bar}$ is similar at different $e_{\rm disk}$, indicating that the detection of strong bars is not biased to the more inclined disks.

In the next sections, we perform checks to verify that the results presented are not dominated by the afore-discussed detection limits. We verify, for instance, that the results over $0.01 \leq z < 0.03$, also hold in the lower redshift bins $0.01 \leq z < 0.02$. We also verify that derived properties of bars hold for bars with a wide range of diameters, and are not biased by the smallest large-scale bars with diameters close or slightly higher 2 kpc, since the latter bars are more susceptible to detection problems.

5. RESULTS

5.1. *The Globally Averaged Optical Bar Fraction and Bar Properties at* $z \sim 0$

As noted in § 2, our sample includes both bright early-type galaxies with bulges, and many disk-dominated galaxies of late Hubble types, while samples in earlier studies (e.g., Eskridge et al. 2000; Elmegreen et al. 2002; Laurikainen et al. 2005, 2006; Buta et al. 2006; MJ07) were dominated by the former group of galaxies. In § 5.2 we investigate the bar properties as a function of different galaxy types, but for now, we begin by estimating globally averaged properties across our full sample.

The optical r-band bar fraction is defined as the fraction of disk galaxies with $i < 60^\circ$ that host large-scale bars, measured on optical images. We find 553 bars among 1144 moderately inclined disk galaxies. Hence, the optical r-band bar fraction, averaged over our sample, which is biased toward late-type disk dominated galaxies, is ~48%. This number could be a lower limit, due to missing weak bars with isophotal twists. As discussed above we found 76 objects with these characteristics, which represent ~7% of the sample. Our result is in good agreement with A. Aguerri et al. (2008, in preparation), who found an optical r-band fraction of ~ 45%, which is also based on SDSS. As stated in § 1, the optical bar fraction is a lower limit to the total bar fraction as the optical images miss bars obscured by dust and

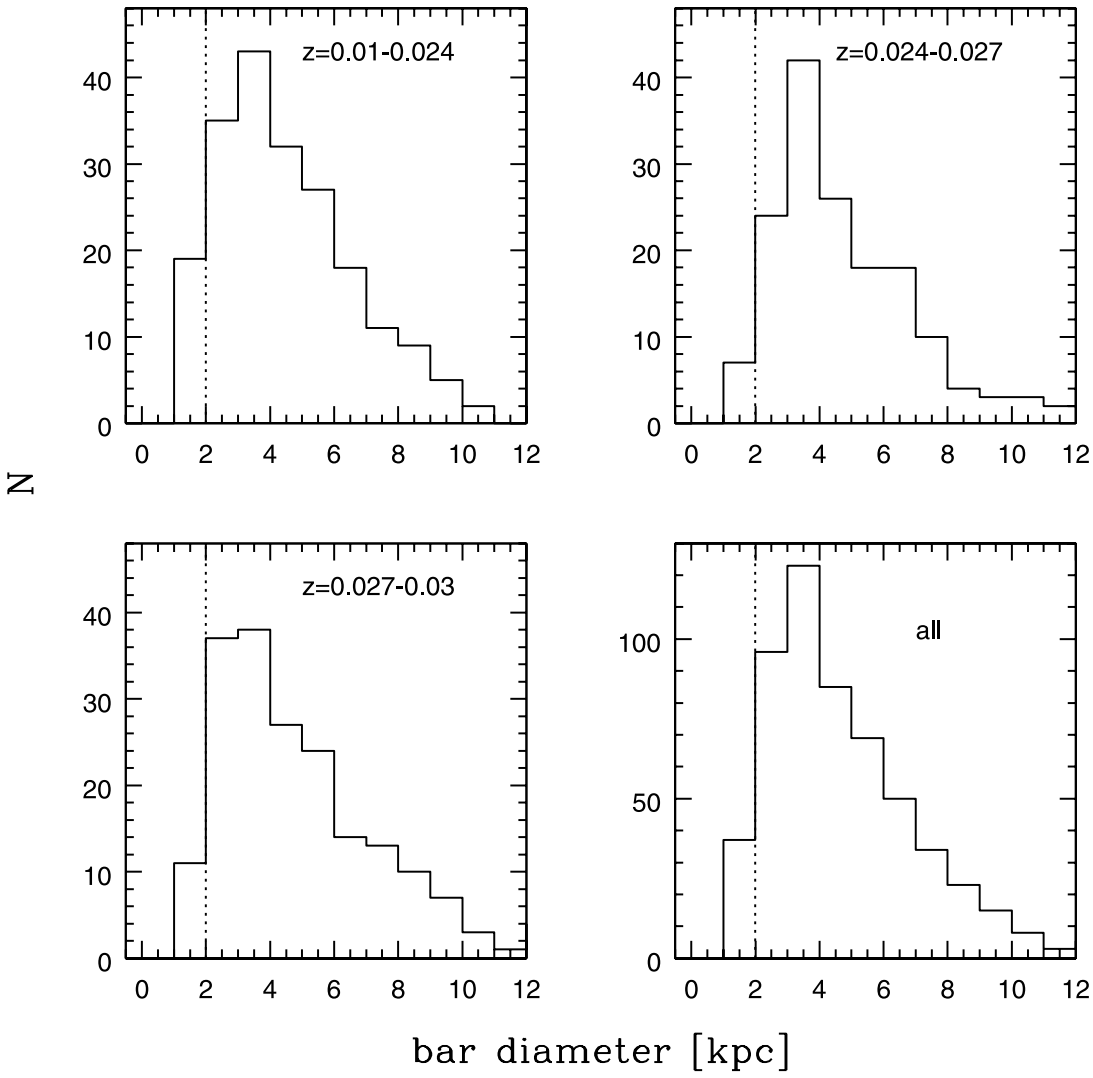

FIG. 9.— Distribution of the bar diameters in three different redshift bins and for the total sample (the bin sizes have been chosen in order to obtain roughly the same number of objects in each bin). The vertical lines indicate the lower limit of 2 kpc for diameters of large-scale bars. The distributions are very similar, in particular we do not miss small bars at higher redshifts.

star formation. Such bars can be detected in the near-infrared and recent studies show that the near-infrared bar fraction is ~15% higher than the optical bar fraction, or around ~60% (MJ07, Laurikainen et al. 2004; Menéndez-Delmestre et al. 2007).

Figure 11*a* shows the distribution of bar semimajor axis lengths for the 553 bars in our sample. We find 37 bars with a semimajor axis <1 kpc, which are commonly considered as nuclear bars, and the remaining are 516 large-scale bars. We exclude the 37 nuclear bars in the following plots and discussions, which affects the optical bar fraction by only ~1%. Most large scale bars (~72%) have sizes in the range 1–3 kpc (Fig. 11*a*). We find relatively few bars with sizes >5 kpc. The median bar size of the sample is 2.2 kpc.

The distributions of bar ellipticities is shown in Figure 11*c*. The majority of bars have ellipticities in the range 0.3–0.7. In general, the distribution is in good agreement with the corresponding *H*-band results of MJ07. We do not find any strong relation between bar ellipticity and absolute magnitude (Fig. 11*d*), or between bar length and absolute magnitude (Figure 11*b*). However, as discussed in § 5.4, the maximum ellipticity or bar strength is on average higher in faint quasi-bulgeless galaxies than in galaxies with bulges (see Fig. 18*d*).

In order to be able to normalize the bar size, we determine the isophotal radius, at which the surface brightness reaches 24 mag arcsec^{-2} (R_{24}). Since we are using *r*-band images, this radius corresponds roughly to R_{25}, the radius, where the *B*-band surface brightness reaches 25 mag arcsec^{-2}. In Figure 12*a* we plot R_{24} versus the bar size. There is no strong correlation between these two parameters, but the bar length is typically much smaller than R_{24}. Figure 12*b* shows the ratio $a_{\rm bar}/R_{24}$ versus the absolute *g*-band magnitude. Most objects have values in the range 0.2–0.4 (median 0.32), which is consistent with the results of MJ07 and Erwin (2005). Theory predicts that the bar ends between the 4:1 and the corotation resonance (CR). Furthermore, studies of the pattern speeds of bars suggest that the bar ends very near the CR, as they find that the ratios between the bar length and the CR are in the range 0.7–0.9 (Aguerri et al. 2003; Debattista & Williams 2004). If these values are representative, then our result that $a_{\rm bar}/R_{24}$ is primarily well below 1, suggests that the CR lies well inside R_{24} in most disks.

5.2. *The Optical Bar Fraction as a Function of Half-Light Radius, r_e/R_{24}, Luminosity, and Color*

The large number of disk galaxies in our sample allows us to perform for the first time a statistically significant study of the

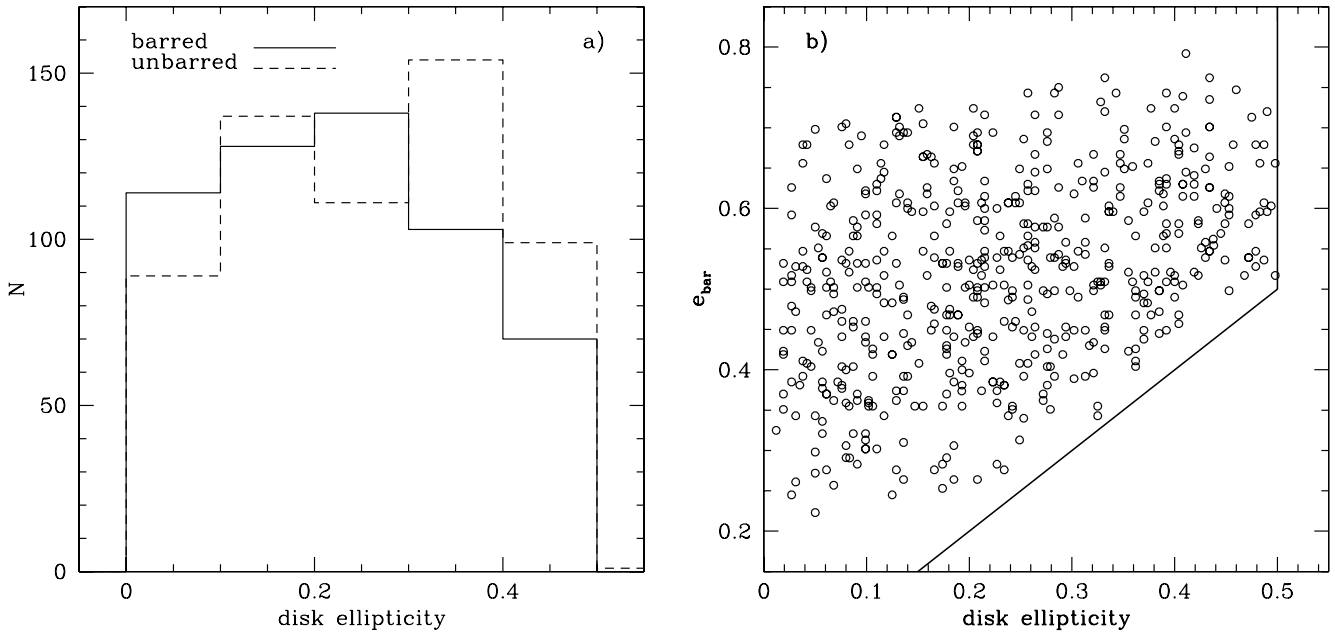

FIG. 10.—(*a*) The disk ellipticities (e_{disk}) of the barred (*solid line*) and unbarred (*dashed line*) subsamples. As e_{disk} varies from 0.0 to 0.5, the total number of barred objects decreases only slightly at $e_{disk} \gtrsim 0.3$. This fall can be attributed to projection effects caused by the inclination of the disk and our criterion (1) for bar detection (see text for details). (*b*) Plot of the disk ellipticity vs. bar ellipticity (e_{bar}) for galaxies classified as barred. The vertical line at e_{disk} of 0.5 reflects the fact that all highly inclined ($i > 60^{\circ}$) disks were excluded from the sample in order to ensure reliable morphological analyzes. The diagonal solid line is defined by $e_{disk} = e_{bar}$. All detected bars lie to the left of this line, reflecting the criterion 1 that the bar ellipticity e_{bar} must be a global maximum. We note that maximum e_{bar} is similar at different e_{disk}, indicating that the detection of strong bars is not biased to the more inclined disks.

dependence of the bar fraction on other galaxy properties, such as luminosity, measures of *B*/*D* ratios, size, colors, surface brightness, etc. In effect, we can bin the data as a function of different parameters with up to 100 galaxies in each bin. We note that this was not possible in earlier studies, which have total sample sizes of $\leq$250 galaxies. Our study can therefore help us understand, which galaxies are more likely to form or maintain a bar and how the presence of a bar relates to the evolution of a galaxy.

For all the results presented in this paper, we omit objects with half light radii $r_e < 2$ kpc. As we show in § 5.4, this regime is strongly contaminated by nondisk galaxies, such as dwarf spheroidals. Without these galaxies the optical *r*-band fraction is 52%. In Figure 13 we show the optical *r*-band bar fraction (f_{opt-r}) as a function of specific galaxy properties. In all panels the numbers next to the points indicate the total number of objects in the corresponding bins. The dashed lines indicate the total optical bar fraction (52%). We only plot bins with more than 10 objects.

Figure 13*a* shows the optical *r*-band bar fraction as a function of the half-light radius (r_e) derived from the single-component two-dimensional Sérsic fit (§ 2). The radius r_e encloses half of the total light of the galaxy and is a measure of the central light concentration of the galaxy. Figure 13*a* shows that the optical bar fraction rises steadily, from ~40%–50% in galaxies with small r_e (2–3 kpc) to ~60% for galaxies with large r_e ($\gtrsim$4 kpc). At a given luminosity, galaxies with a large *B*/*D* ratio typically have a smaller r_e than disk-dominated galaxies with no bulge or only a very low *B*/*D*. At this point, one may be tempted to ask whether the drop in the optical *r*-band bar fraction in Figure 13*a*, as r_e drops from 4 to 2 kpc, is due to the bar being too small to be detected. This is not the case because *r_e is not equivalent to the size of the disk or bar component*. In particular, galaxies with a large *B*/*D* and low r_e may have an extended disk and a large bar. This is shown in Figures 14*a* and 14*b*, where r_e is plotted against the bar semi major axis a_{bar} for 2 redshift bins. It is evident that for $r_e \sim 2$–4 kpc, a_{bar} ranges from 1 to 5 kpc, and is easily resolved. Thus, the trend in optical bar fraction with r_e in Figure 13*a* seems to be a solid one. We further investigate this below using r_e/R_{24}.

In Figure 13*b* we plot the optical bar fraction as a function of the normalized r_e, using R_{24} as normalization. At a given luminosity, r_e/R_{24} is a measure of the relative light distribution in the bulge and disk, and hence a rough measure of the *B*/*D* light ratio. The ratio r_e/R_{24} is not correlated to M_g (not shown). Fig. 13*b* is very similar to Figure 13*a*, also showing a steep increase of the bar fraction toward larger, more extended galaxies. In fact, the effect is more pronounced in Figure 13*b*, where the optical bar fraction reaches only ~30% for the most compact disks and rises to more than 60% for the most extended disks. This shows that the increase in bar fraction is not primarily a luminosity effect, but is related to the structure of the disk. Therefore, Figure 13*b* can be interpreted as indicating that the *optical bar fraction is higher in disk-dominated systems*. Visual classification, as discussed in detail in § 5.4, confirms this interpretation.

In Figure 13*c*, f_{opt-r} is roughly constant at $M_g < -19.5$ mag (neglecting the brightest bin, which is very small) and increases toward the fainter end of the magnitude range, reaching almost 60% for the faintest bin. This is consistent with the above interpretation of a higher bar fraction in disk-dominated galaxies, since the latter dominate at fainter magnitudes.

In Figure 13*d* we plot the optical *r*-band bar fraction as a function of $g - r$ color. Notice the sharp increase in bar fraction as the $g - r$ color gets bluer from 0.55 to 0.30. There are two potential interpretations of this trend. One interpretation is that star-forming galaxies host an excess of bars (e.g., Hunt & Malkan 1999) as the star formation is bar-induced. However, looking at the *g*-band images of our sample galaxies, we do not find that barred late-type disks show more centrally concentrated star formation than unbarred galaxies. Another more likely interpretation is that the higher optical bar fraction in late-type, disk-dominated galaxies, suggested by Figure 13*b*, naturally leads to a higher optical bar fraction for bluer colors, because late-type galaxies tend to be

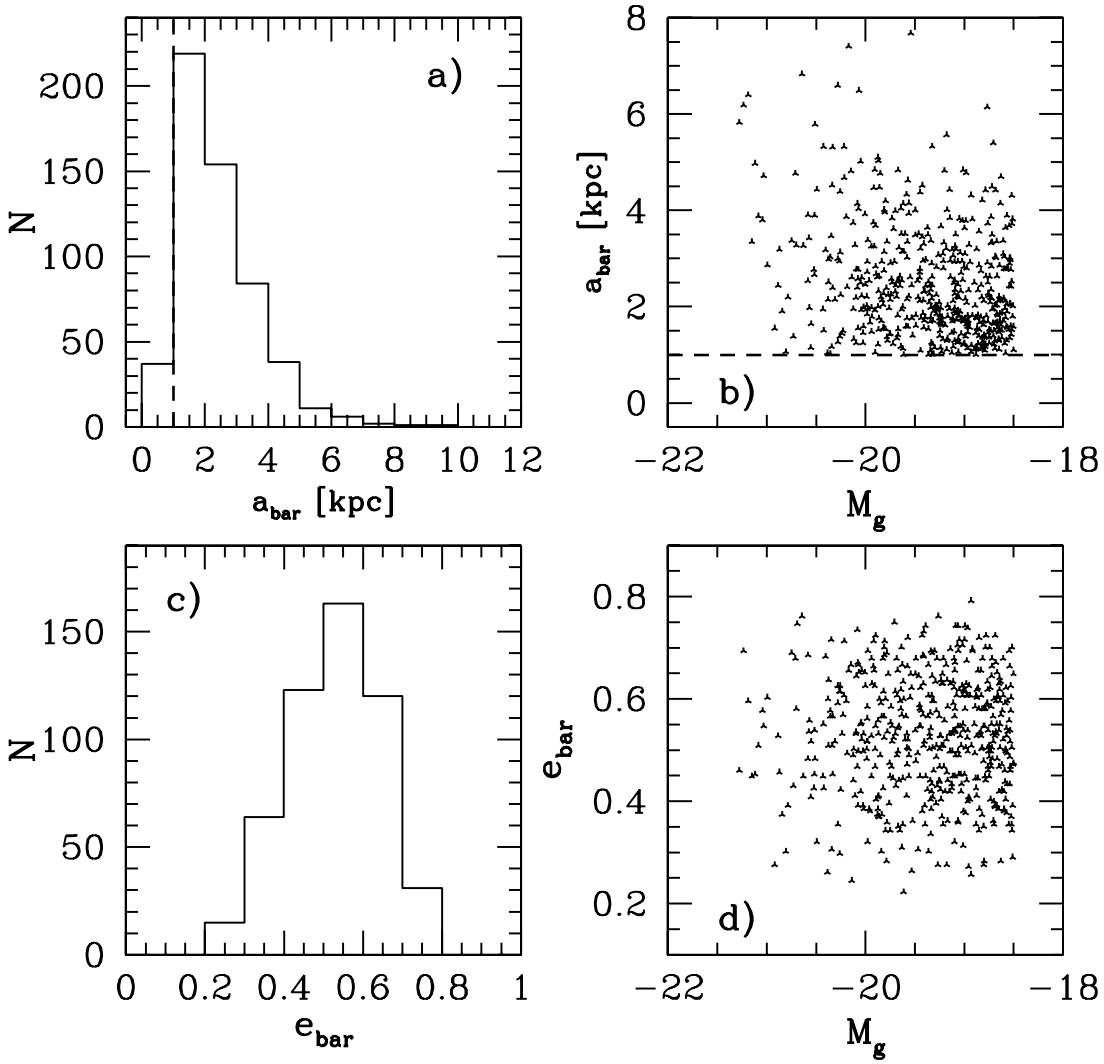

FIG. 11.—(*a*) Distribution of bar semimajor axis lengths. We find very few bars with sizes >5 kpc. (*b*) Plot showing absolute *g*-band magnitude vs. bar semimajor axis. (*c*) The distribution of bar ellipticities. Most bars have ellipticities in the range 0.3–0.7. (*d*) Absolute *g*-band magnitude vs. bar ellipticity showing no obvious relation.

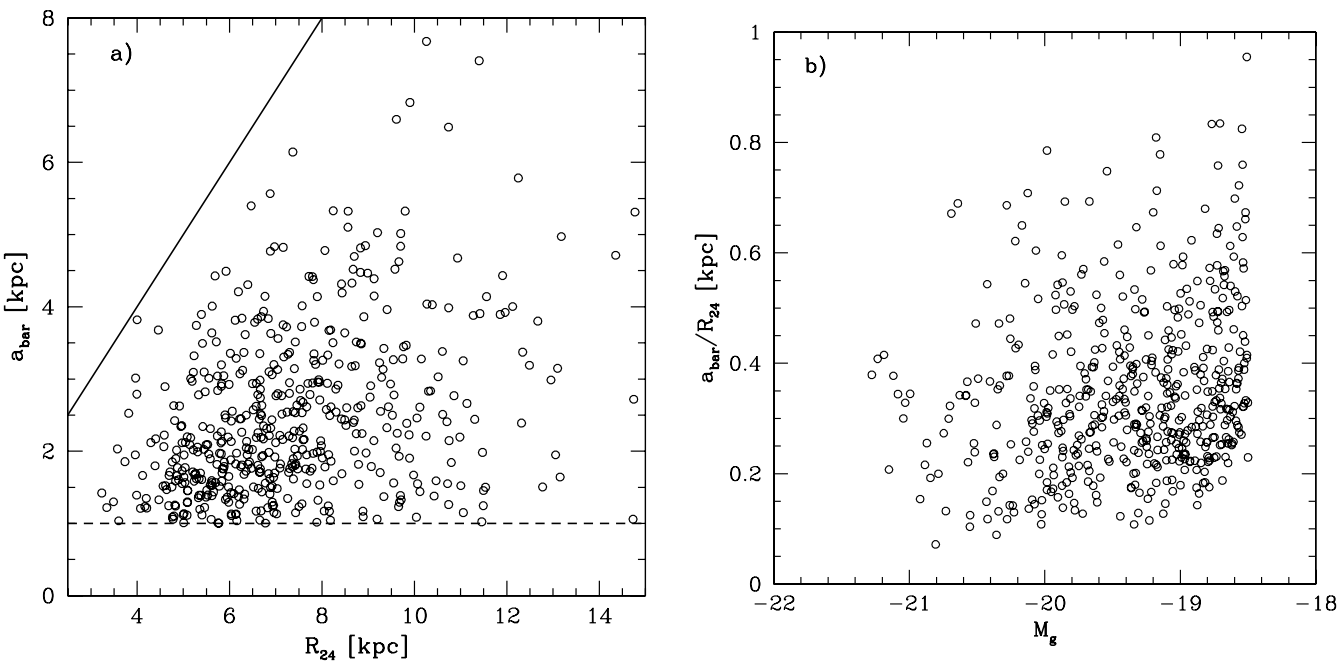

FIG. 12.—(*a*) Plot of the bar semimajor axis vs. R_{24}. The solid line indicates $x = y$. There is no clear correlation between these two parameters, but the bar typically ends inside R_{24}. (*b*) Absolute *g*-band magnitude vs. the ratio a_{bar}/R_{24}. Most galaxies have ratios in the range 0.2–0.4 (median 0.32).

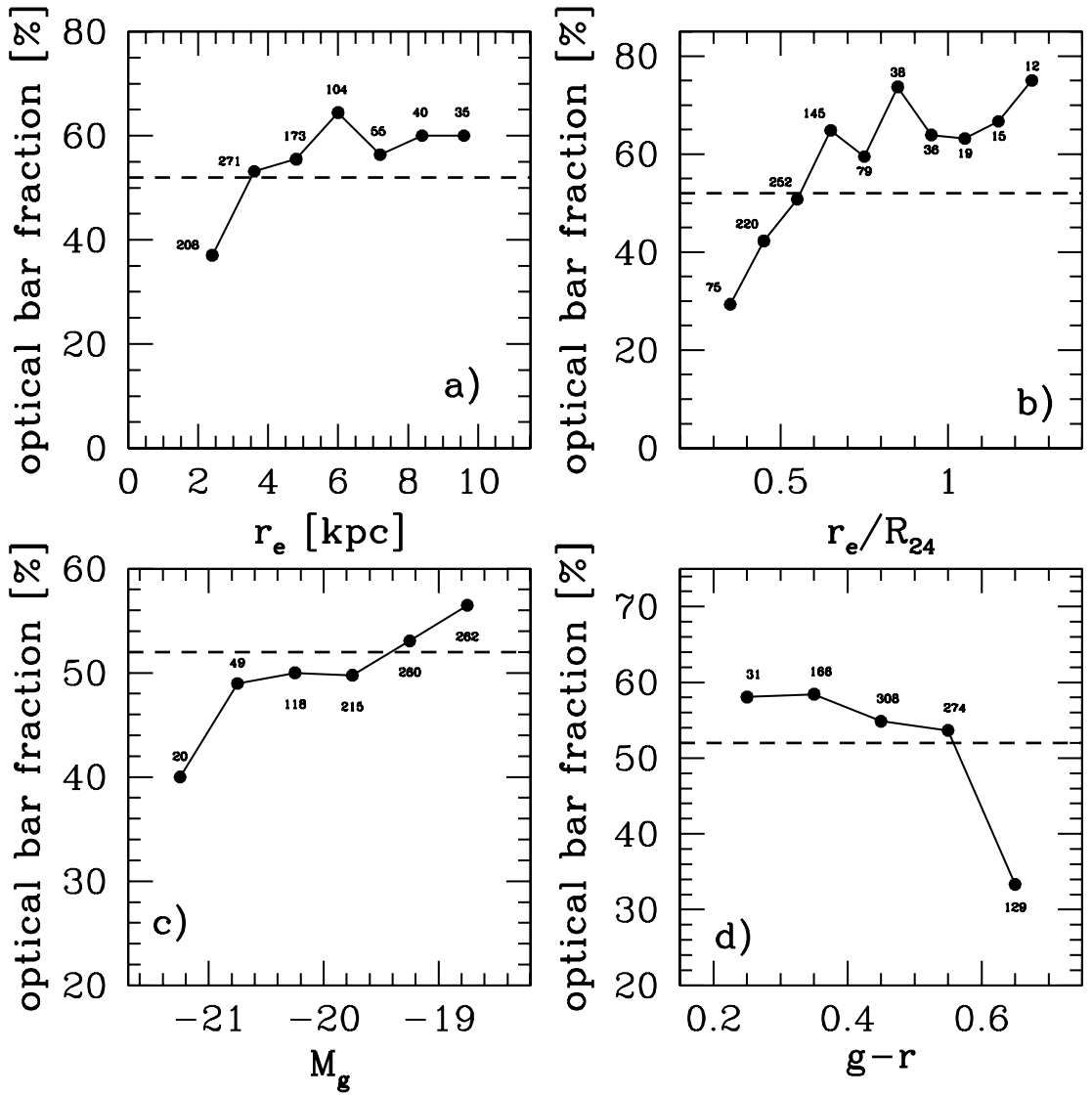

FIG. 13.—Optical r-band bar fraction ($f_{\mathrm{opt}-r}$) as a function of different galaxy properties. In all panels the numbers next to the points indicate the number of galaxies in the corresponding bins. The dashed lines indicate the total optical bar fraction (52%). We only show bins with more than 10 objects. (*a*) The optical bar fraction as a function of half light radius r_e: $f_{\mathrm{opt}-r}$ rises sharply, from ~40% in galaxies that have small r_e and visually appear bulge-dominated, to ~60% for galaxies that have large r_e ($\gtrsim 4$ kpc) and appear disk-dominated. (*b*) The optical bar fraction as a function of normalized r_e/R_{24}. The smallest (or most compact) galaxies have a bar fraction of ~30%, whereas the largest (most extended) galaxies reach a value of ~70%. (*c*) The optical bar fraction as a function of absolute g-band magnitude: $f_{\mathrm{opt}-r}$ is roughly constant at $M_g < -19.5$ mag (neglecting the brightest bin, which is very small) and increases toward the fainter end of the magnitude range, reaching almost 60% for the faintest bin. (*d*) The optical bar fraction as a function of $g - r$ color: Notice the sharp increase in bar fraction toward bluer colors.

bluer and have higher specific star formation rates (Gavazzi et al. 1998; Bendo et al. 2002; Koopmann & Kenney 2004). The analysis in § 5.6 and Figure 20 further support this interpretation.

The fact that the relationship between optical bar fraction and blue colors has not been reported in earlier studies (MJ07; Eskridge et al. 2000) is likely due to the fact that their samples were dominated by brighter earlier-type galaxies, while ours has a large number of late-type disk-dominated galaxies (§ 2).

5.3. *The Optical Bar Fraction as a Function of n and μ_0*

In Figure 15*a* we plot $f_{\mathrm{opt}-r}$ as a function of the Sérsic index n. The low $f_{\mathrm{opt}-r}$ for $n > 2.5$ are likely due to blue spheroids contaminating the color-selected sample of disk galaxies (see also Fig. 2). The rise in $f_{\mathrm{opt}-r}$ at $n \leq 1.5$ is consistent with a larger bar fraction in disk-dominated systems.

In order to further investigate the assumption that the bar fraction is related to the presence and size of a bulge, we measure the central surface brightnesses (μ_0) of the galaxies directly on the r-band images. This is an important test as the measurement of μ_0 provides a measure of the central light concentration, which is *model-independent* and not affected by the bar itself. In contrast, the half light radius r_e was derived from a Sérsic fit, and it is possible that parameters, such as r_e or R_{24}, are affected by the details of the fit or the presence of a bar. For instance, bars dominating the light distribution in disks could automatically lead to larger r_e and R_{24}, because they efficiently disperse the luminosity. This would, however, only be the case in galaxies, where the bar is much more luminous than the bulge and the underlying disk. We measured μ_0 on the same physical size (1 kpc^2) for all galaxies. In Figure 15*b* we plot the optical bar fraction as a function of μ_0. The bar fraction is steadily rising for decreasing μ_0. This result is similar to the ones for r_e and r_e/R_{24}. However, the change of the bar fraction with respect to μ_0 is less steep, but more continuous. This result lends support to the view that

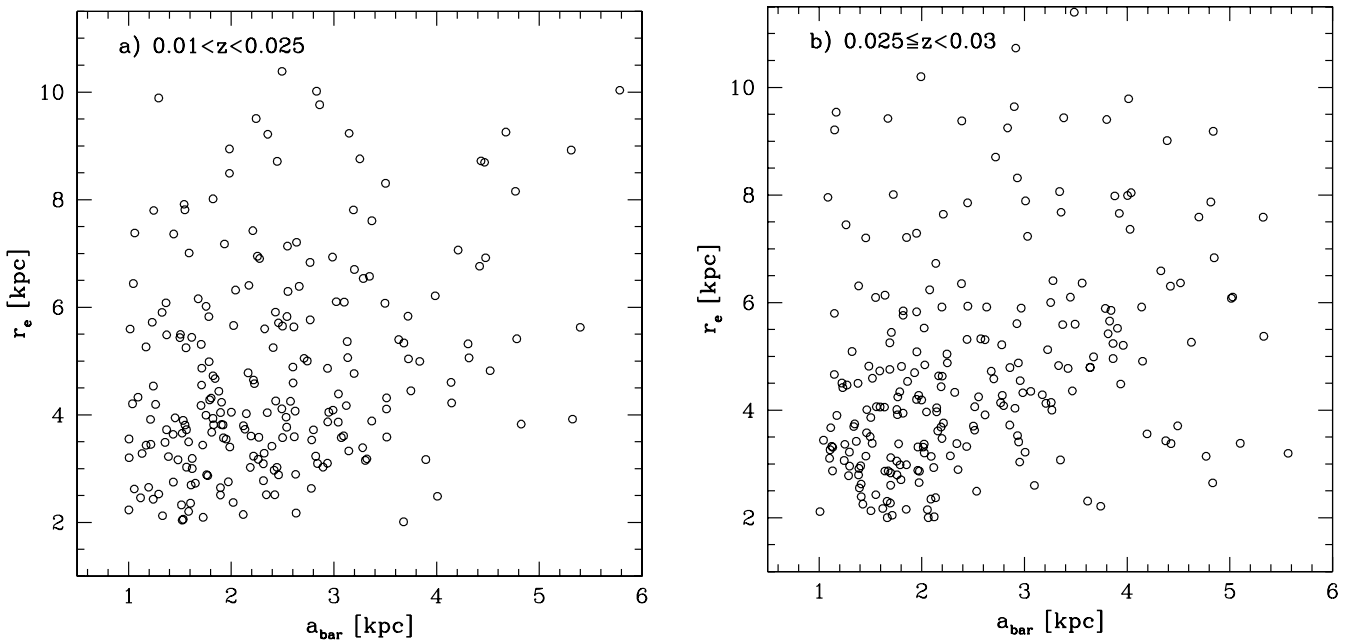

FIG. 14.—Two plots showing the absolute bar size ($a_{\rm bar}$) vs. r_e for two redshift bins, (*a*) $0.01 < z < 0.025$ and (*b*) $0.025 \leq z < 0.03$. The two distributions are very similar and indicate that the bars in galaxies with small r_e cover the whole range of bar sizes.

bars are more likely to be found in disks with relatively small bulges.

5.4. *Visual Classifications of Disk-dominated versus Early-Type Galaxies*

In § 5.2 and 5.3, we interpreted the higher optical bar fraction at larger r_e (Fig. 13*a*) and r_e/R_{24} (Fig. 13*b*) as meaning that disk-dominated galaxies with very low B/D ratio have a higher optical bar fraction. The most rigorous way to test this claim is to perform three- component bulge+bar+disk decomposition on the two-dimensional light distribution of the galaxy, and derive a B/D. However, this task is beyond the scope of the present paper. Instead, we perform a first-order test by visually classifying ~80% of our sample, which includes galaxies with r_e in the range 2–10 kpc. Our main goal in this visual classification is to identify late-type disk-dominated galaxies with no significant bulge, as well as early-type galaxies with bulge and disk components, so that we can compare their bar fractions. We also classify the subgroup of systems with $r_e < 2$ kpc, which we excluded from our sample in § 5.2, on the ground that this group is strongly contaminated by pure bulge/spheroidal galaxies, such as dwarf spheroidals or dwarf ellipticals. A secondary goal of the visual

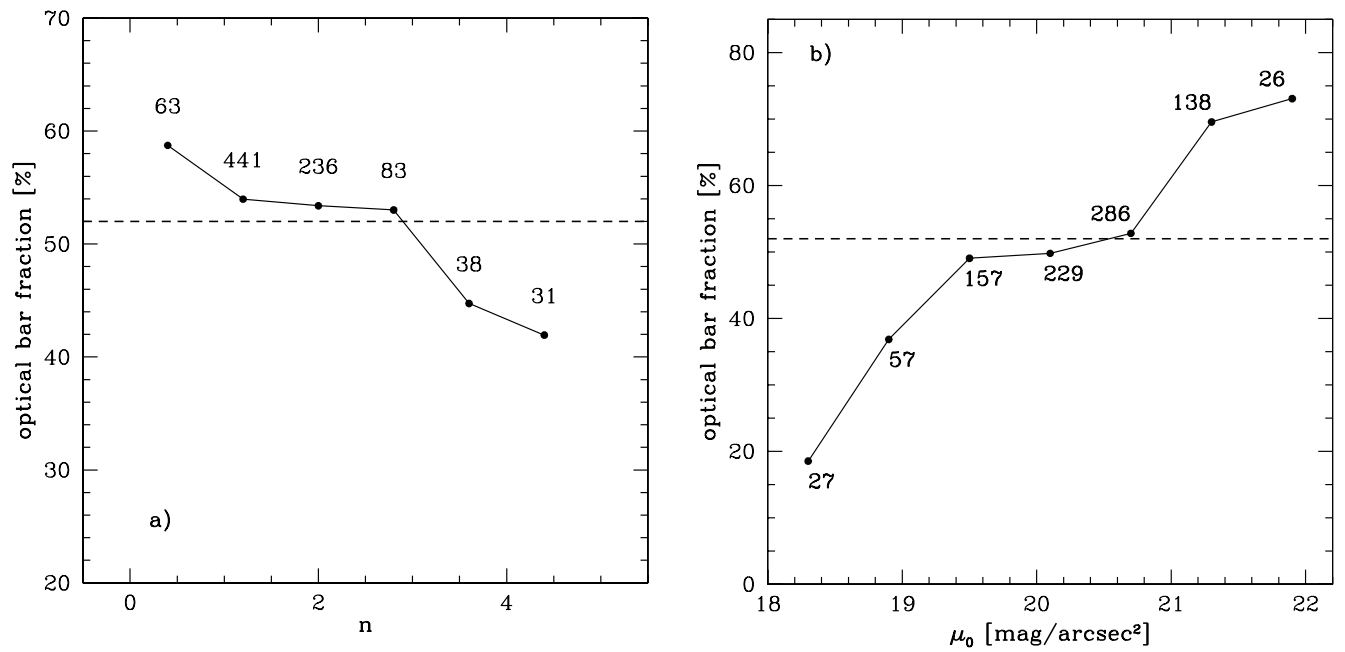

FIG. 15.—(*a*) Optical bar fraction as a function of n: the low $f_{\rm opt-r}$ for $n > 2.5$ are likely due to blue spheroids contaminating the color-selected sample of disk galaxies. The rise in $f_{\rm opt-r}$ at $n \leq 1.5$ is consistent with a larger bar fraction in disk-dominated systems. (*b*) The optical bar fraction as a function of μ_0. The numbers in the plot and the dashed line have the same meaning as in Fig. 13. The increase of the bar fraction is not as steep as in the plot of r_e and r_e/R_{24}, but changes more continuously.

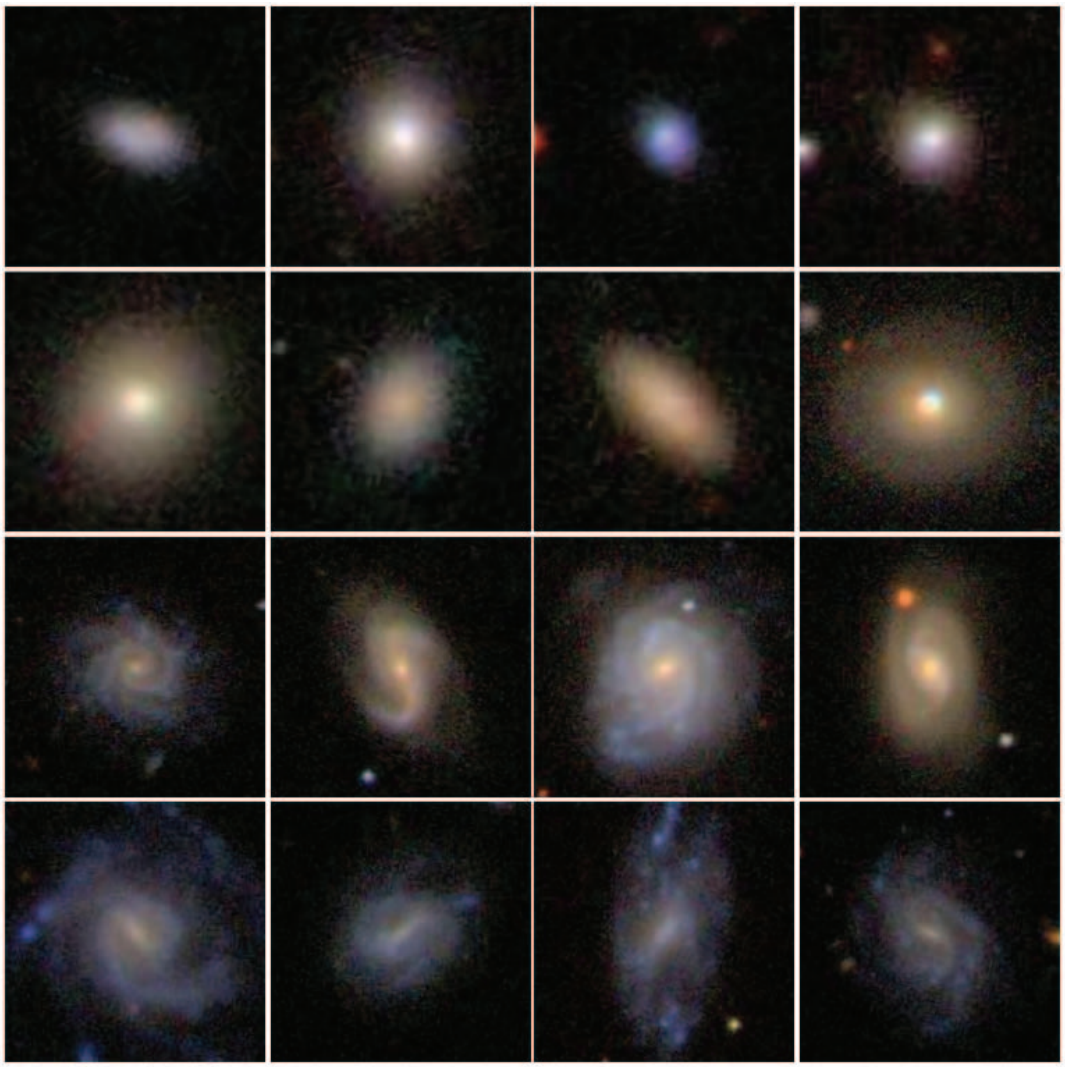

FIG. 16.—Three band (g, r, i) color images from the SDSS archive for 16 objects from the test sample. The first row shows examples of objects, which have been classified as pure spheroids (class 1), the second and third rows show examples of objects with disk+bulge (class 2), and the four row shows pure disks (class 3). The first seven images (*from top and left to right*) have a size of $25'' \times 25''$ and the remaining nine have $50'' \times 50''$.

classification is to identify pure bulge systems and verify that they indeed cluster at $r_e < 2$ kpc.

Visual inspection does not allow one to classify galaxies in fine grids of B/D ratios, but it does allow one to reliably classify galaxies into three broad visual classes (VCs):

Class 1.—Pure bulge or spheroid; steady decrease of the surface brightness from the center outward, with no obvious break in the surface brightness profile.

Class 2.—Disk galaxy with bulge.

Class 3.—Pure disk with no bulge; no bright, distinct, and roughly round central object.

The classification has been performed by all three authors, making sure that each object is classified by at least two classifiers. A small fraction of the objects have been classified twice to test the robustness of the results. The agreement between classifiers is very good (>80%), and the final result represents an average of all classifications. In Figure 16 we show images of 16 representative objects. The galaxies in the first row have been classified as pure spheroids (class 1), objects in row two and three are in class 2, and the fourth row shows examples of pure disks (class 3).

The first result of our visual classification is that our sample of 1144 disk galaxies (with $i < 60^\circ$), which was color selected (§ 2), only has a small contamination of ~7% by pure spheroids (class 1). Many of these objects in class 1 are relatively blue and faint. These objects could be dwarf ellipticals, which experienced a recent episode of star formation and whose luminosity is therefore dominated by rather blue stars. It is also interesting to note that almost all of these objects have $n < 2.5$ and would also have been included in our sample of disk galaxies if we had used a Sérsic cut to select the sample (e.g., see Fig. 2). The main point to note is that the small fraction (~7%) of class 1 objects would not have any significant impact on our globally averaged results, such as the global optical bar fraction (§ 5.1). However, the contamination particularly affects the results in the lowest $r_e < 2$ kpc bin as ~95% of the class 1 (pure spheroids) objects are very compact and fall in this bin. This results in a spheroid contamination of up to 20% for objects with $r_e < 2$ kpc, which makes the bar fraction for this subsample very uncertain. Thus, throughout this paper (§ 5.2 onward), we excluded all objects with $r_e < 2$ kpc from the plots and subsequent analysis. We estimate that the contamination by spheroids for the remaining sample is <1%.

Next, we discuss the galaxies that are visually classified as class 2 (bulge+disk) and class 3 (bulgeless) galaxies. In the sample of 886 galaxies with $r_e > 2$ kpc, ~20% of galaxies fall in class 3 (bulgeless), while the remaining fall in class 2. It is remarkable

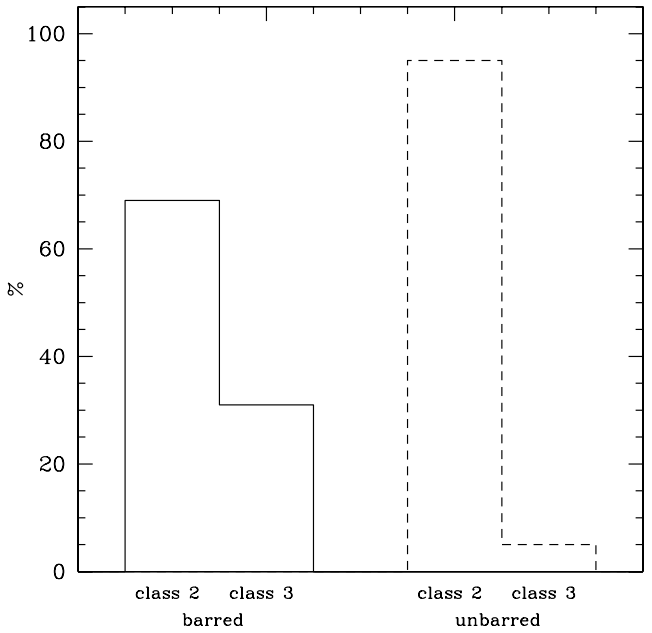

FIG. 17.—Histograms showing the percentage of class 3 (bulgeless) and class 2 (bulge+disk) galaxies among barred galaxies (*solid histogram*) and unbarred galaxies (*dashed histogram*). The fraction of bulgeless galaxies in much higher (31% vs. 5%) in barred than unbarred systems.

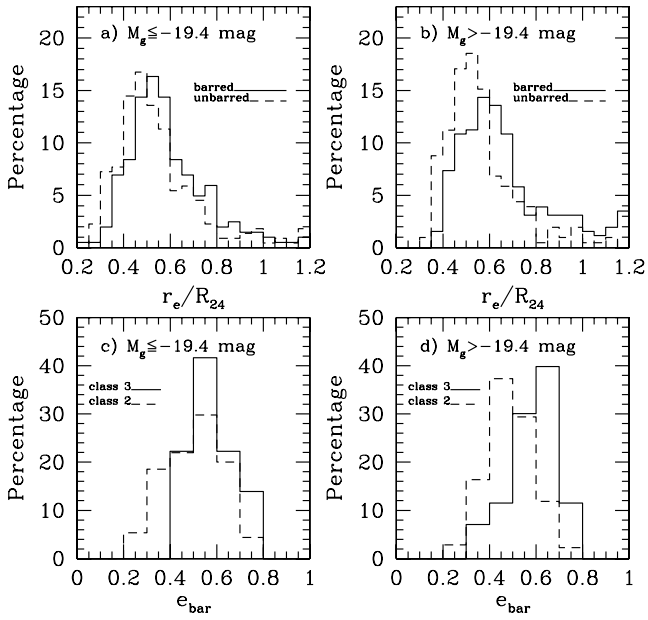

FIG. 18.—(*a*, *b*) Distribution of r_e/R_{24} among barred galaxies (*solid histogram*) and unbarred galaxies (*dashed histogram*) for (*a*) the brighter galaxies and (*b*) the fainter galaxies. The fraction of galaxies with large r_e/R_{24} ratios is higher in barred than unbarred systems, particularly among the fainter galaxies. (*c*, *d*) The distribution of $e_{\rm bar}$ among galaxies in class 3 (bulgeless; *solid histogram*) and galaxies in class 2 (bulge+disk; *dashed histogram*) for (*c*) the brighter galaxies and (*d*) the fainter galaxies. The $e_{\rm bar}$ distributions in panel *d* indicate that bar ellipticities or strengths are on average higher in faint disk-dominated galaxies than in bulge-dominated galaxies.

that *the optical bar fraction of the class 3* (*bulgeless*) *disk galaxies is ∼87%, compared to ∼44% for class 2* (*bulge+disk*) *galaxies.* This striking difference supports the basic conclusion of § 5.2 and 5.3: *disk-dominated galaxies with no bulge or a very low B/D display a much higher optical bar fraction than galaxies with significant bulges*. In fact, it appears that a pure disk is twice as likely to be barred than a disk galaxy with a bulge. We note that the higher bar fraction found for class 3 objects is also consistent with the high bar fractions in late-type galaxies reported by Odewahn (1996) and Elmegreen et al. (2004a) based on RC3 visual bar classes and RC3 Hubble types.

Another way to illustrate the results is to look at the difference in disk properties between barred and unbarred galaxies. Figure 17 shows the percentage of class 3 (bulgeless) and class 2 (bulge+disk) galaxies among barred galaxies (*solid histograms*) and unbarred galaxies (*dashed histogram*). The fraction of bulgeless galaxies in much higher (31% vs. 5%) in barred than unbarred systems. Figures 18*a* and 18*b* show the distributions of r_e/R_{24} among barred galaxies (*solid histograms*) and unbarred galaxies (*dashed histograms*) for galaxies brighter than the median luminosity of the sample (*a*) and for galaxies fainter than the median (*b*). The fraction of galaxies with large r_e/R_{24} ratios is higher in barred than unbarred systems, particularly for the fainter subsample. Figures 18*c* and 18*d* show the distributions of bar ellipticities for galaxies in class 3 (*solid histograms*) and galaxies in class 2 (*dashed histograms*), again for the bright and faint subsamples. These figures indicate that the bars in bulge-dominated galaxies are generally weaker than in disk-dominated galaxies. It seems that the presence of a bulge weakens the bar, in particular in fainter galaxies (panel *d*). However, one has to keep in mind that $e_{\rm bar}$ has been determined including the bulges and that the measured bar ellipticities may be affected by the bulges, in the cases where the end of the bar is close to the bulge.

In summary, the visual classifications have provided two important results. They show that the contamination from non–disk galaxies is small and confined to the regime $r_e < 2$ kpc. These galaxies do not impact our result as the regime $r_e < 2$ kpc is excluded from all analysis in this paper. Second, and more importantly, the visual classifications support the claim, made in §§ 5.2 and 5.3, that disk-dominated galaxies with a very low *B*/*D* display a significantly higher optical bar fraction (60%–70%) than galaxies with a significant bulge (40%–50%). The associated ramifications are discussed in § 6.

5.5. *The Bar Fraction as a Function of Mass*

The mass of galaxy disks is one of the fundamental parameters controlling their evolution. We use the prescription of Bell et al. (2003) to derive stellar mass-to-light ratios using the $g - r$ color:

$$\log(M/L_r) = -0.306 + 1.097(g - r)$$

This mass-to-light ratio is then used to derive the stellar masses of the galaxies using the following relation:

$$\log(M) = \log(M/L_r) - 0.4(M_r - r_\odot),$$

where $r_\odot = 4.67$ is the absolute *r*-band magnitude of the Sun.

The optical bar fraction as a function mass is shown in Figure 19. Over the mass range 5×10^9 to 5×10^{10} $M_\odot$, the optical bar fraction rises for lower masses. This trend is expected from our earlier findings (§§ 5.2 and 5.3) of a higher optical bar fraction in galaxies, which are more disk-dominated, less centrally concentrated, bluer, and fainter.

5.6. *Which Disk Parameters Most Strongly Influence the Optical Bar Fraction?*

In § § 5.2–5.5, we showed that the optical bar fraction rises with lower bulge-to-disk ratios, as characterized visually (Fig. 17) and also via r_e/R_{24} (Fig. 13*b*), with lower central surface brightness

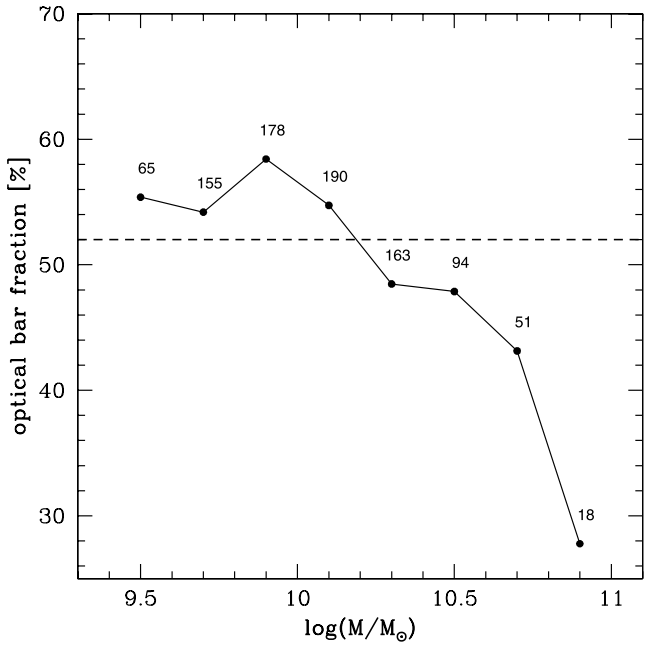

FIG. 19.—Optical r-band bar fraction as a function of galaxy mass. The masses have been determined using the $g - r$ color and the prescription of Bell et al. (2003).

(Fig. 15*b*) and with bluer $g - r$ colors (Fig. 13*d*). There is also a weaker trend with fainter absolute magnitude M_g (Fig. 13*c*) and with lower masses (Fig. 19).

Many of these parameters are correlated and the above findings are all consistent with the optical bar fraction rising toward late-type galaxies (e.g., Sd, Sm). The latter systems have no bulge or very low bulge-to-disk ratios, low central mass concentrations, and are on average fainter, bluer, and less massive than early-type galaxies.

Here we investigate whether the trends in optical fraction with r_e/R_{24} hold, even when some of the other properties, such as absolute magnitude M_g, $g - r$ color, Sérsic index n, and mass, are not allowed to vary significantly. To this effect, we split our sample into two subgroups according to the median values of M_g (Fig. 20*a*), $g - r$ color (Fig. 20*b*), Sérsic index n (Fig. 20*c*), and mass (Fig. 20*d*). We then plot the optical bar fraction as a function of r_e/R_{24} in each of the two subgroups, as shown in Figures 20*a*–20*d*. The filled circles indicate bins with more than 20 objects, whereas the open circles represent bins with less than 20 objects.

The optical bar fraction does not show any systematic variation between the bright and faint subsamples at a given r_e/R_{24} (Fig. 20*a*). A similar result is seen with respect to mass (Fig. 20*d*), and color (Fig. 20*b*). This shows that even for samples with a narrow range in mass, color, or luminosity, the trend of rising optical fraction with larger r_e/R_{24} (i.e., lower bulge-to-disk ratio) remains strong.

Figure 20*c* shows a significant difference in optical bar fraction between the subsamples separated by Sérsic index n. At a given r_e/R_{24}, the optical bar fraction is systematically higher, typically by more than 20%, for the subsample with the lower Sérsic index $n \leq 1.48$ (Fig. 20*c*). Since the Sérsic index n is low in pure disk galaxies, this result supports our suggestion that disk-dominated galaxies with a very low B/D display a significantly higher optical bar fraction than galaxies with prominent bulges. The potential implications of such a relation on bar formation and disk stability are discussed in § 6.

6. DISCUSSION

6.1. *Implication for Bulge Formation Models*

Hierarchical Λ cold dark matter (CDM) models (e.g., Somerville & Primack 1999; Cole et al. 2000; Steinmetz & Navarro 2002) provide a good description of how dark matter (DM) behaves on large scales. By modeling the baryonic component and feedback processes, predictions can be made regarding the disk, bulge, and bar components of galaxies. In such models, gas with low angular momentum settles in the central parts of CDM halos to form small and dense protodisks (e.g., White & Rees 1978; D'Onghia & Burkert 2004). Subsequent mergers of these central stellar disks lead to classical spheroidal bulges with a de Vaucouleurs $r^{1/4}$ profile (e.g., Steinmetz & Navarro 2002; Taylor & Babul 2003). It is also conceivable that the bulge does not form in a single event, but is assembled by star-forming clumps, which originate in a protodisk and coalesce in the center of the disk and form a bulge (Noguchi 1999; Immeli et al. 2004). This possibility has gained support by the observation of disk galaxies with prominent clumps at high redshift (Elmegreen et al. 2004b). The later accretion of high angular momentum gas around this bulge invariably produces a spiral galaxy with a classical bulge and an extended disk. In major mergers of spirals, violent relaxation destroys the disks to produce an elliptical galaxy, while minor mergers with mass ratios above 1:4 typically spare the disk.

While observations support many aspects of hierarchical ΛCDM models, the latter face several challenges. In particular, many cosmological simulations with a merger history inclusive of major mergers fail to produce galaxies without classical bulges (e.g., Burkert & D'Onghia 2004; D'Onghia et al. 2006), while high-resolution simulations of assembling disks with feedback from stellar energy (e.g., Heller et al. 2007) seem to reproduce a range of bulge-dominated to bulgeless disks. In this context, our study finds that in the range $-18.5 \leq M_g < -22.0$ mag and redshift $0.01 \leq z < 0.03$, $\sim 20\%$ of the 900 disk galaxies that are visually classified appear to be "quasi-bulgeless," without a classical bulge. A similar fraction of 15% for bulgeless galaxies was reported in the study of inclined disks by Kautsch et al. (2006).

Another aspect of bulge formation not usually addressed by hierarchical models is the formation of disky bulges with high v/σ (or "pseudobulges"). There are significant differences between classical bulges and disky bulges. While classical bulges form by gravitational collapse or hierarchical merging, disky bulges are believed to form through gas inflows triggered by bars or any other nonaxisymmetric feature in the gravitational potential (Kormendy 1993; Kormendy & Kennicutt 2004; Jogee et al. 2005; Debattista et al. 2006). Classical bulges are typically an order of magnitude more massive than disky ones and therefore also brighter and larger. Furthermore, studies of the stellar populations of classical bulges indicate that their stars have been formed very quickly and long ago (Peletier et al. 1999). Our results show that more bars are present in late-type disks where typically disky "pseudobulges" lie, a fact consistent with a bar-driven origin for "pseudobulges."

6.2. *Implications for Disk Stability and Bar Formation Scenarios*

One of the main results of our study is that the optical bar fraction rises from ~45% in early-type galaxies to a significantly higher value (≥70%) in late-type galaxies, which appear quasi-bulgeless, and seem to have a low B/D ratio, as measured by r_e/R_{24}, and confirmed by visual inspection. The optical bar fraction shows a similar but shallower trend with mass, rising in

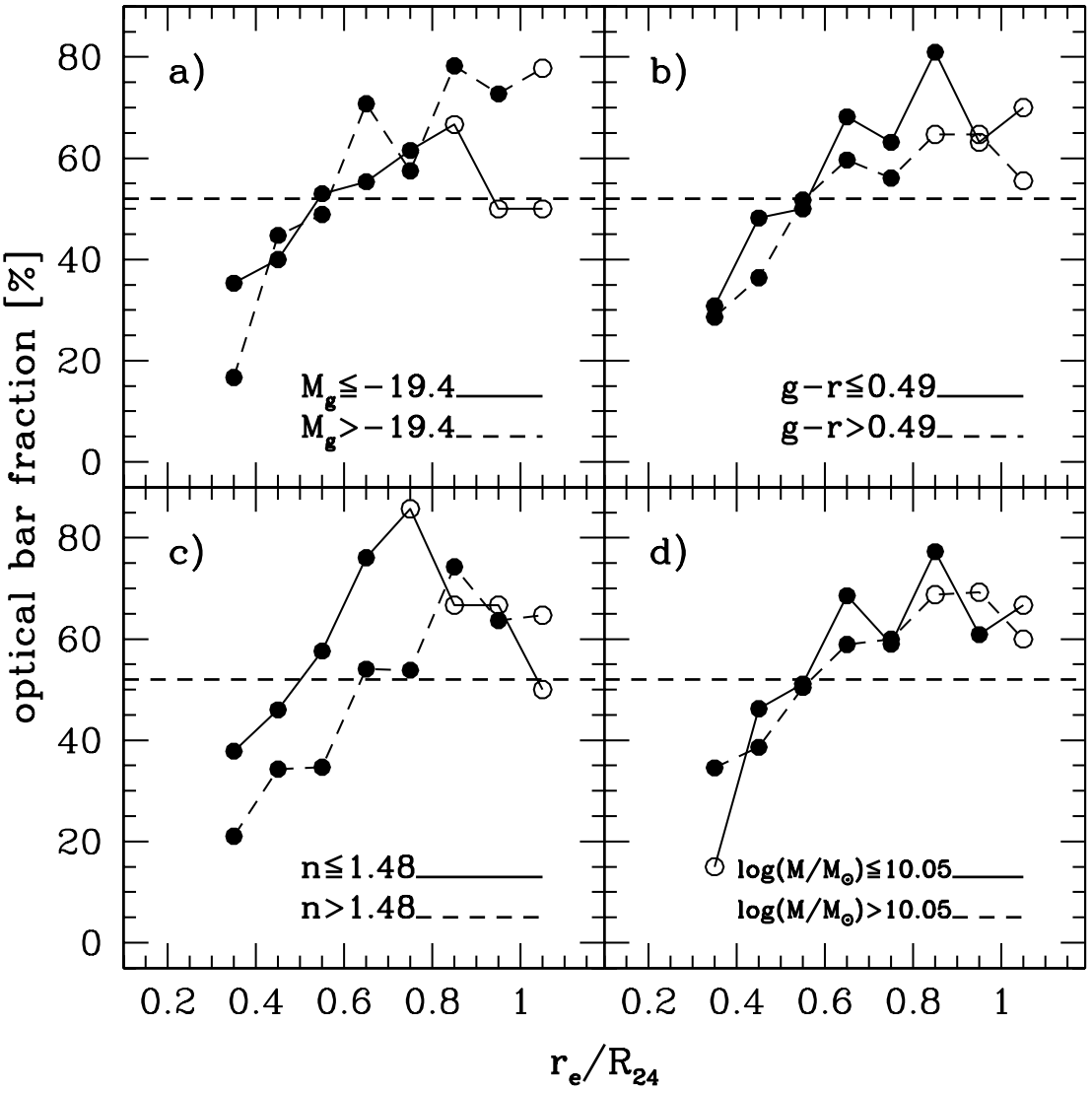

FIG. 20.—Optical bar fraction as a function of r_e/R_{24} for different subsamples defined according to the median values of basic galaxy properties. The split locations are indicated in the four panels. The solid points denote bins with more than 20 objects, whereas the open points represent bins with less than 20 objects. The dashed lines indicate the total optical bar fraction (52%). The sample has been split based on (*a*) absolute *g*-band magnitude, (*b*) $g-r$ color, (*c*) Sérsic index *n*, and (*d*) galaxy mass.

low-mass galaxies (Fig. 19). Our conclusion is also supported by Odewahn (1996), who finds that the frequency of bars roughly doubles from Sc to Sm galaxies, using the RC3 bar classifications and Hubble types.

In this section we discuss how our findings can be interpreted in the context of bar formation scenarios. As one moves from early-/intermediate-type galaxies (e.g., Sa to Sc) to late-type (e.g., Sd, Sm) systems, several important properties change: the gas mass fraction in the disk rises, the *B*/*D* ratio falls, and the total mass falls. In addition, it is also found that the DM fraction rises in lower luminosity systems (e.g., Persic et al. 1996; Kassin et al. 2006), but the scatter in such relations is large (Kassin et al. 2006). How do these changes along the Hubble sequence impact the susceptibility of a disk to form bars and the subsequent bar evolution?

The higher gas mass fraction present in late-type disks makes the disk dynamically cold and lowers the Toomre Q parameter (Toomre 1964), defined as

$$Q = \frac{\kappa\sigma}{\pi G \Sigma_{\rm disk}},$$

where $\Sigma_{\rm disk}$ is the disk mass surface density, σ is the gas velocity dispersion, and κ is the epicyclic frequency. A low Q (e.g., ≤ 2–3) favors the onset of bar instabilities and allows strong amplification in the context of the swing amplifier (Binney & Tremaine 1987).

It has been proposed that the swing amplifier (Julian & Toomre 1966; Toomre 1981; Binney & Tremaine 1987) model may be relevant for bar formation. In such a scenario, a bar forms via a resonant cavity of swing amplifying spiral density waves that reflect off the center and the corotation radius. One way to suppress bar formation in this model is to introduce an inner Lindblad resonance (ILR), which absorbs the spiral density waves, thereby killing the feedback loop. In fact, Sellwood & Evans (2001) find that a disk with a sharp central density is completely stable to bar formation. In the context of the swing amplifier, a late-type galaxy with a low *B*/*D* ratio would have a shallow rotation curve, and may not harbor an ILR, thus favoring bar formation.

The DM halo can have a large impact on the growth of a bar. The early work of Ostriker & Peebles (1973) suggested that the presence of a dynamically important unresponsive DM halo can suppress the bar instability in a disk galaxy. However, the evolution of a bar is a highly nonlinear process, which depends on

the exchange of angular momentum with the outer disk and the DM halo via resonances (e.g., Weinberg 1985; Athanassoula 2002, 2003; Debattista & Sellwood 1998, 2000; Berentzen et al. 2006, 2007). Work with live halos has showed that there is resonant transfer of angular momentum between the bar, the DM halo, and the outer disk (e.g., Debattista & Sellwood 1998, 2000; Athanassoula 2002, 2003): the angular momentum absorbed by the DM halo makes an existing bar grow and slow down. In fact, in the simulations with live halos of Athanassoula (2002) a strong bar grows even in disks whose DM halo mass within the optical radius exceeds that of the disk mass. It should also be noted that even if the dark matter only becomes important outside the bar radius, it can still interact with outer resonances in the bar potential, causing the bar to grow. Thus, it appears that the larger dark matter fraction in late-type disks would favor the growth of a bar, if one already exists. It still remains unclear, however, whether a massive DM halo would promote the formation of a bar in the case of an unbarred disk. Furthermore, the shape of the DM halo (triaxial or axisymmetric) also has an important impact (e.g., Berentzen et al. 2006, 2007). We also note that cosmological simulations of galactic disks (e.g., Governato et al. 2007; Heller et al. 2007) show extensive bar-forming activity, but there has not been any specific prediction of how the bar fraction would vary as a function of Hubble type.

It is also important to consider whether our results could be explained in terms of the evolution and destruction of bars rather than their initial formation. Most simulations (Shen & Sellwood 2004; Athanassoula et al. 2005; Martinez-Valpuesta et al. 2006; Debattista et al. 2006) indicate that *present-day* bars are relatively robust against the type of central mass concentrations (CMCs) and *B*/*D* that exist in *present-day* galaxies today or in the recent past (see also the discussion in § 6.3). Specifically, as outlined in Athanassoula et al. (2005) and Shen & Sellwood (2004) the supermassive black holes (SMBHs), central, dense stellar clusters, gaseous concentrations, and inner parts of bulges, which exist in present-day galaxies, fail significantly to generate the required CMCs for bar destruction. This does not exclude, however, the possibility that at very early epochs (e.g., $z > 1.5$) when disks were still assembling, the different prevailing physical conditions (e.g., large CMCs and gas inflows) might destroy bars (e.g., Bournaud et al. 2005, but see Debattista et al. 2006; Heller et al. 2007). Lenses, which are preferentially found in early-type disks (Kormendy 1979; Kormendy & Kennicutt 2004), are sometimes interpreted as dissolving bars. Within this framework, our results of a higher optical bar fraction of bars in quasi-bulgeless, late-type galaxies may reflect the fact that bars in early-type galaxies were destroyed more frequently during their earlier assembly. We note that in our study, the bar maximum ellipticity is on average higher in faint quasi-bulgeless galaxies than in galaxies with bulges (Fig. 18*d*).

6.3. *Implication for the Evolution of Bars over the Last* 8 Gyr *in Bright Galaxies*

The evolution of the optical bar fraction with redshift is a subject of active study. Early small studies reported that the optical fraction of bars shows a striking decline at $z >\sim 0.5$ (Abraham et al. 1999), and undergoes a dramatic order-of-magnitude decline from ∼29% to below 1% (van den Bergh et al. 2000).

Subsequent studies (Jogee et al. 2004; Elmegreen et al. 2004a; Sheth et al. 2003; Zheng et al. 2005) ruled out a dramatic order-of-magnitude decline, and reported a fairly constant optical fraction of strong bars or prominent bars (∼23%–30%) over $z = 0.2$–1.0 (look-back times of 3–8 Gyr). The results of such studies allowed, within the error bars, for modest factors of ∼2 variation in the optical fraction of strong bars or of all bars. For example, for bright ($M_V < -19.3$) disks, Jogee et al. (2004) find a rest-frame optical fraction of strong ($e_{\rm bar} \geq 0.4$) bars of $\sim 36\% \pm 6\%$ at $z \sim 0.2$–0.7, and $\sim 24\% \pm 4\%$ at $z \sim 0.7$–1.0, allowing a range of 42%–20% for the optical fraction of strong bars, and yielding an average values of ∼30%. A similar result was found for the completeness cut of $M_V < -20.6$ (Jogee et al. 2004). However, not much weight was given to a possible factor of ∼2 variation due to the small number statistics and due to redshift-dependent systematic effects that may cause an artificial loss of optical bars in the higher redshift bins. These include the increasing obscuration by dust and star formation, with the average star formation rate increasing by a factor of ∼4 over $z \sim 0.2$ to 0.8 (Jogee et al. 2008), the degradation of the PSF (0.09″) from 300 to 680 pc, and the surface brightness dimming by a factor of 5 from $z \sim 0.2$ to 0.8.

Recent studies using COSMOS data (Sheth et al. 2007) with a significantly larger sample of bright (massive ($M \geq 10^{10}\ M_\odot$) galaxies report a moderate decline by a factor of 2 or 3 in the optical fraction of strong bars (from 30%–35% at $z \sim 0.2$ to 9%–17% at $z \sim 0.8$). They also report a decline in the optical fraction of (strong+weak) bars from ∼60% at $z \sim 0$ to ∼22%–31% at $z \sim 0.8$. If this decline is not caused by the afore mentioned redshift-dependent systematic effects, it implies that the frequency of both strong and weak bars is lower at earlier times.

We can compare our globally averaged optical bar fraction at $z \sim 0$ (§ 5.1) to the results at intermediate redshifts, but it is critical to note two things. First, these studies are carried out in the rest-frame *optical* band and therefore should be compared to the *optical* bar fraction at $z \sim 0$. Second, comparisons should be made for galaxies of the same luminosity or/and mass range.

We first compare the SDSS results with the study by Jogee et al. (2004) on strong bars, where they find a rest-frame optical fraction of strong ($e_{\rm bar} \geq 0.4$) bars of $\sim 36\% \pm 6\%$ at $z \sim 0.2$–0.7, and $\sim 24\% \pm 4\%$ at $z \sim 0.7$–1.0. If we restrict our sample to galaxies with $M_g \leq -19.3$ mag and only consider bars that are strong (ellipticity ≥0.4) and large enough (semimajor axis ≥1.5 kpc) to be characterized via ellipse-fitting out to $z \sim 0.8$, we get an optical *r*-band fraction for strong bars of ∼34%. (For $M_g \leq -20.6$, a value of 31% is obtained, but number statistics are low and based on only 54 galaxies.) The value of 34% is only slightly higher, by a factor of 1.4, compared to the value of $\sim 24\% \pm 4\%$ seen in the higher redshift bin ($z \sim 0.7$–1.0) of the Jogee et al. (2004) study. Thus, we find that once the loss of bars due to poor resolution is taken into account, the data are consistent with the optical fraction of strongly barred galaxies suffering at most a decline by a factor of ∼1.4 out to $z \sim 1$. In fact, as discussed in MJ07, if one assumes a further modest loss of optical bars due to increasing obscuration, the data may even allow for a rise in the total fraction of strong bars out to $z \sim 1$.

The study by Sheth et al. (2007) focuses on massive and bright galaxies, with masses in the range 1×10^{10} to $1 \times 10^{11}\ M_\odot$, and M_V in the range −21.2 to −23.7 mag. The SDSS sample of 2000 disk galaxies over $z = 0.01$–0.03 has very few such bright galaxies (Figs. 3 and 13*c*), and thus a comparison over the same luminosity range is not possible. However, we can compare the optical bar fraction over the mass range 1×10^{10} to $3 \times 10^{10}\ M_\odot$, where the SDSS and Sheth et al. (2007) data overlap. The SDSS-based optical bar fraction over this mass range is ∼47% over $z \sim 0.01$–0.03. This is similar to the value of ∼60% in the first redshift bin ($z \sim 0.17$–0.37) of the Sheth et al. (2007) study. If we consider only bars that are large enough (semimajor axis >1.5 kpc) to be reliably characterized via ellipse-fitting out to $z \sim 0.8$, the SDSS-based optical bar fraction falls from ∼47% to ∼39%. For

comparison, the optical bar fraction is ~25% in the last bin ($z \sim 0.60$–0.84). Thus, once the loss of bars due to poor resolution is taken into account, the observed value of ~25% is consistent with the optical bar fraction declining by at most a factor of (39%/25%) or ~1.6 over this mass range.

7. SUMMARY AND CONCLUSIONS

We have used the *r*-band images from the NYU-VAGC of a sample of 3692 galaxies with $-18.5 \leq M_g < -22.0$ mag and redshift $0.01 \leq z < 0.03$ to find and characterize bars. While most studies of bars in the local universe have been based on relatively small samples that are dominated by bright early-type (Sa to Sc) galaxies with bulges, the present sample also includes many galaxies that are disk-dominated and of late Hubble types. Furthermore, the sample is ~10 times larger and samples a larger volume than earlier local samples We used a color cut in the color-magnitude diagram to select ~2000 disk galaxies. We cross-check that Sérsic cuts would yield a similar sample. We identify and characterize bars and disks using *r*-band images and a method based on ellipse fits and quantitative criteria. The typical seeing (1.4″ or 290–840 pc over $0.01 \leq z < 0.03$) is adequate for resolving large-scale bars, whose typical diameters are ≥2 kpc. Smaller nuclear bars are not the focus of this study. After the standard procedure of excluding highly inclined (>60°) systems, we find the following results.

1. The average optical *r*-band bar fraction ($f_{\mathrm{opt}-r}$) in our sample, which primarily consists of late-type disk-dominated galaxies, is ~48%–52%. The bars have diameters *d* of 2 to 24 kpc, with most (~72%) having $d \sim 2$–6 kpc (Fig. 11*a*). The bar length is typically much smaller than R_{24} (Fig. 12*a*) and most galaxies have a a_{bar}/R_{24} in the range 0.2–0.4 (Fig. 12*b*).

2. When galaxies are separated according to normalized r_e/R_{24}, which is a measure of the *B*/*D* ratio, a remarkable result is seen: the optical *r*-band fraction rises sharply, from ~40% in galaxies that have small r_e/R_{24} and visually appear bulge-dominated, to ~70% for galaxies that have large r_e/R_{24}. Visual classification of ~80% of our sample (with $i < 60°$) confirms our result that *late-type disk-dominated galaxies with no bulge or a very low B/D display a significantly higher optical bar fraction (>70% vs. 40%) than galaxies with prominent bulges.* It also shows that barred galaxies host a larger fraction (31% vs. 5%) of quasi-bulgeless disk-dominated galaxies than do unbarred galaxies. The bar ellipticities or strengths are on average higher in faint disk-dominated galaxies than in bulge-dominated galaxies (Fig. 18*d*).

3. Similar trends in the optical bar fraction are found using the central surface brightness and color. Bluer galaxies have higher bar fractions (~58% at $g - r = 0.3$) than the redder objects (~32% at $g - r = 0.65$) (Fig. 13*d*). The optical *r*-band fraction also shows a slight rise for galaxies with fainter luminosities (Fig. 13*c*) and lower masses (Fig. 19). This is expected from (2), given that late-type galaxies are fainter, bluer, and less massive.

4. The significant rise in the optical bar fraction toward disk-dominated galaxies is discussed in terms of their higher gas mass fraction, higher DM fraction, and lower bulge-to-disk ratio.

5. While many hierarchical ΛCDM models of galaxy evolution models fail to produce galaxies without classical bulges, our study finds that in the range $-18.5 \leq M_g < -22.0$ mag and redshift $0.01 \leq z < 0.03$, ~20% of the 1144 moderately inclined disk galaxies appear to be "quasi-bulgeless," without a classical bulge.

6. Our study of bars at $z \sim 0$ in the optical *r* band provides a reference $z \sim 0$ baseline for intermediate-redshift *HST* ACS surveys that trace bars in *bright* disks in the rest-frame optical bands (*BVRI*) out to $z \sim 1$. By applying the same cutoffs in magnitude, bar ellipticity ($e_{\mathrm{bar}} \geq 0.4$), and bar size ($a_{\mathrm{bar}} \geq 1.5$ kpc), which are applied in $z \sim 0.2$–1.0 studies in order to trace strong bars with adequate spatial resolution in bright disks, we obtain an optical *r*-band fraction for strong bars of 34%. This is comparable to the values of ~30% at $z \sim 0.2$–1.0, ~36% ± 6% at $z \sim 0.2$–0.7, and ~24% ± 4% at $z \sim 0.7$–1.0. Our result implies that the optical fraction of strong bars in bright galaxies does not suffer any dramatic order-of-magnitude decline out to $z \sim 1$.

F. D. B. and S. J. acknowledge support from the National Aeronautics and Space Administration (NASA) LTSA grant NAG5-13063 and from HST-GO-10395 and HST-GO-10428. S. J. and I. M. acknowledge support from the NSF grant AST 06-07748. We thank Isaac Shlosman, Juntai Shen, Lia Athanassoula, Victor Debattista, Francoise Combes, Bruce Elmegreen, and Alfonso Aguerri for useful discussions. This research has made use of NASA's Astrophysics Data System Service.

REFERENCES

Abazajian, K., et al. 2004, AJ, 128, 502
Abraham, R. G., Merrifield, M. R., Ellis, R. S., Tanvir, N. R., & Brinchmann, J. 1999, MNRAS, 308, 569
Aguerri, J. A. L., Debattista, V. P., & Corsini, E. M. 2003, MNRAS, 338, 465
———. 1992a, MNRAS, 259, 328
———. 1992b, MNRAS, 259, 345
———. 2002, ApJ, 569, L83
———. 2003, MNRAS, 341, 1179
———. 2005, MNRAS, 358, 1477
Athanassoula, E., Lambert, J. C., & Dehnen, W. 2005, MNRAS, 363, 496
Barden, M., et al. 2005, ApJ, 635, 959
Bell, E. F., McIntosh, D. H., Katz, N., & Weinberg, M. D. 2003, ApJS, 149, 289
Bell, E. F., et al. 2004a, ApJ, 608, 752
———. 2004b, ApJ, 600, L11
Bendo, G. J., et al. 2002, AJ, 124, 1380
Berentzen, I., Shlosman, I., & Jogee, S. 2006, ApJ, 637, 582
Berentzen, I., Shlosman, I., Martinez-Valpuesta, I., & Heller, C. 2007, ApJ, 666, 189
Binney, J., & Tremaine, S. 1987, Galactic Dynamics (Princeton: Princeton Univ. Press)
Blanton, M. R., et al. 2005, AJ, 129, 2562
Block, D. L., Bournaud, F., Combes, F., Puerari, I., & Buta, R. 2002, A&A, 394, L35
Bournaud, F., Combes, F., & Semelin, B. 2005, MNRAS, 364, L18
Bureau, M., & Athanassoula, E. 2005, ApJ, 626, 159
Bureau, M., & Freeman, K. C. 1999, AJ, 118, 126
Burkert, A. M., & D'Onghia, E. 2004, Penetrating Bars Through Masks of Cosmic Dust, ed. D. L. Block et al. (Dordrecht: Kluwer), 341
Buta, R., Laurikainen, E., Salo, H., Block, D. L., & Knapen, J. H. 2006, AJ, 132, 1859
Buta, R., Vasylyev, S., Salo, H., & Laurikainen, E. 2005, AJ, 130, 506
Cole, S., Lacey, C. G., Baugh, C. M., & Frenk, C. S. 2000, MNRAS, 319, 168
Combes, F., Debbasch, F., Friedli, D., & Pfenniger, D. 1990, A&A, 233, 82
Combes, F., & Sanders, R. H. 1981, A&A, 96, 164
Contopoulos, G., & Papayannopoulos, T. 1980, A&A, 92, 33
Debattista, V. P., Mayer, L., Carollo, C. M., Moore, B., Wadsley, J., & Quinn, T. 2006, ApJ, 645, 209
Debattista, V. P., & Sellwood, J. A. 1998, ApJ, 493, L5
———. 2000, ApJ, 543, 704
Debattista, V. P., & Williams, T. B. 2004, ApJ, 605, 714
de Vaucouleurs, G., de Vaucouleurs, A., Corwin, H. G., Jr., Buta, R. J., Paturel, G., & Fouqué, P. 1991 (Berlin: Springer)
D'Onghia, E., & Burkert, A. 2004, ApJ, 612, L13
D'Onghia, E., Burkert, A., Murante, G., & Khochfar, S. 2006, MNRAS, 372, 1525
Elmegreen, B. G. 1994, ApJ, 425, L73
Elmegreen, B. G., Elmegreen, D. M., & Hirst, A. C. 2004a, ApJ, 612, 191

Elmegreen, D. M., Elmegreen, B. G., Frogel, J. A., Eskridge, P. B., Pogge, R. W., Gallagher, A., & Iams, J. 2002, AJ, 124, 777
Elmegreen, D. M., Elmegreen, B. G., & Hirst, A. C. 2004b, ApJ, 604, L21
Erwin, P. 2005, MNRAS, 364, 283
Eskridge, P. B., et al. 2000, AJ, 119, 536
———. 2002, ApJS, 143, 73
Friedli, D., Wozniak, H., Rieke, M., Martinet, L., & Bratschi, P. 1996, A&AS, 118, 461
Gavazzi, G., Catinella, B., Carrasco, L., Boselli, A., & Contursi, A. 1998, AJ, 115, 1745
Giavalisco, M., et al. 2004, ApJ, 600, L93
Governato, F., Willman, B., Mayer, L., Brooks, A., Stinson, G., Valenzuela, O., Wadsley, J., & Quinn, T. 2007, MNRAS, 374, 1479
Heller, C., Shlosman, I., & Athanassoula, L. 2007, ApJ, 671, 226
Hunt, L. K., & Malkan, M. A. 1999, ApJ, 516, 660
Immeli, A., Samland, M., Gerhard, O., & Westera, P. 2004, A&A, 413, 547
Jogee, S., Kenney, J. D. P., & Smith, B. J. 1999, ApJ, 526, 665
Jogee, S., Knapen, J. H., Laine, S., Shlosman, I., Scoville, N. Z., & Englmaier, P. 2002a, ApJ, 570, L55
Jogee, S., Scoville, N., & Kenney, J. D. P. 2005, ApJ, 630, 837
Jogee, S., Shlosman, I., Laine, S., Englmaier, P., Knapen, J. H., Scoville, N., & Wilson, C. D. 2002b, ApJ, 575, 156
Jogee, S., et al. 2004, ApJ, 615, L105
Jogee, S., et al. 2008, in ASP Conf. Ser., Formation and Evolution of Galaxy Disks, ed. J. G. Funes & E. M. Corsini (San Francisco: ASP), in press
Julian, W. H., & Toomre, A. 1966, ApJ, 146, 810
Kassin, S. A., de Jong, R. S., & Weiner, B. J. 2006, ApJ, 643, 804
Kautsch, S. J., Grebel, E. K., Barazza, F. D., & Gallagher, J. S., III 2006, A&A, 445, 765
Knapen, J. H. 1999, in ASP Conf. Ser. 187, The Evolution of Galaxies on Cosmological Timescales, ed. J. E. Beckman & T. J. Mahoney (San Francisco: ASP), 72
Knapen, J. H., Beckman, J. E., Heller, C. H., Shlosman, I., & de Jong, R. S. 1995, ApJ, 454, 623
Knapen, J. H., Shlosman, I., & Peletier, R. F. 2000, ApJ, 529, 93
Koopmann, R. A., & Kenney, J. D. P. 2004, ApJ, 613, 851
———. 1979, ApJ, 227, 714
Kormendy, J. 1993, in IAU Symp. 153, Galactic Bulges, ed. H. DeJonghe & H. J. Habing (Dordrecht: Kluwer), 209
Kormendy, J., & Kennicutt, R. C., Jr. 2004, ARA&A, 42, 603
Kuijken, K., & Merrifield, M. R. 1995, ApJ, 443, L13
Laine, S., Shlosman, I., Knapen, J. H., & Peletier, R. F. 2002, ApJ, 567, 97
Laurikainen, E., Salo, H., & Buta, R. 2004, ApJ, 607, 103
———. 2005, MNRAS, 362, 1319
Laurikainen, E., Salo, H., Buta, R., Knapen, J., Speltincx, T., & Block, D. 2006, AJ, 132, 2634
Laurikainen, E., Salo, H., & Rautiainen, P. 2002, MNRAS, 331, 880
Marinova, I., & Jogee, S. 2007, ApJ, 659, 1176 (MJ07)
Martinez-Valpuesta, I., Shlosman, I., & Heller, C. 2006, ApJ, 637, 214
McIntosh, D. H., et al. 2005, ApJ, 632, 191
Menéndez-Delmestre, K., Sheth, K., Schinnerer, E., Jarrett, T. H., & Scoville, N. Z. 2007, ApJ, 657, 790
Noguchi, M., 1999, ApJ, 514, 77
Odewahn, S. C. 1996, in IAU Colloq. 157, Barred Galaxies, ed. R. Buta, D. A. Crocker, & B. G. Elmegreen (ASP Conf. Ser. 91; San Francisco: ASP), 30
Ostriker, J. P., & Peebles, P. J. E. 1973, ApJ, 186, 467
Peletier, R. F., Balcells, M., Davies, R. L., Andredakis, Y., Vazdekis, A., Burkert, A., & Prada, F. 1999, MNRAS, 310, 703
Peng, C. Y., Ho, L. C., Impey, C. D., & Rix, H. 2002, AJ, 124, 266
Persic, M., Salucci, P., & Stel, F. 1996, MNRAS, 281, 27
Reese, A. S., Williams, T. B., Sellwood, J. A., Barnes, E. I., & Powell, B. A. 2007, AJ, 133, 2846
Regan, M. W., & Teuben, P. J. 2004, ApJ, 600, 595
Rix, H.-W., et al. 2004, ApJS, 152, 163
Scoville et al. 2007, ApJS, 172, 1
Sellwood, J. A., & Evans, N. W. 2001, ApJ, 546, 176
Shen, J., & Sellwood, J. A. 2004, ApJ, 604, 614
Sheth, K., Menendez-Delmestre, K., Scoville, N., Jarrett, T., Strubbe, L., Regan, M. W., Schinnerer, E., & Block, D. L. 2004, in Penetrating Bars through Masks of Cosmic Dust, ed. D. L. Block et al. (Dordrecht: Kluwer), 405
Sheth, K., Regan, M. W., Scoville, N. Z., & Strubbe, L. E. 2003, ApJ, 592, L13
Sheth, K., Regan, M. W., Vogel, S. N., & Teuben, P. J. 2000, ApJ, 532, 221
Sheth, K., Vogel, S. N., Regan, M. W., Thornley, M. D., & Teuben, P. J. 2005, ApJ, 632, 217
Sheth, K., et al. 2007, preprint (arXiv: 0710.4552)
Somerville, R. S., & Primack, J. R. 1999, MNRAS, 310, 1087
Steinmetz, M., & Navarro, J. F. 2002, NewA, 7, 155
Taylor, J. E., & Babul, A. 2003, Ap&SS, 284, 405
Toomre, A. 1964, ApJ, 139, 1217
———. 1981, in Structure and Evolution of Normal Galaxies, ed. S. F. Fall & D. Lynden-Bell (Cambridge: Cambridge Univ. Press), 111
Tran, H. D., et al. 2003, ApJ, 585, 750
van den Bergh, S., Cohen, J. G., Hogg, D. W., & Blandford, R. 2000, AJ, 120, 2190
Weinberg, M. D. 1985, MNRAS, 213, 451
White, S. D. M., & Rees, M. J. 1978, MNRAS, 183, 341
Wolf, C., Gray, M. E., & Meisenheimer, K. 2005, A&A, 443, 435
Whyte, L. F., Abraham, R. G., Merrifield, M. R., Eskridge, P. B., Frogel, J. A., & Pogge, R. W. 2002, MNRAS, 336, 1281
Zheng, X. Z., Hammer, F., Flores, H., Assémat, F., & Rawat, A. 2005, A&A, 435, 507